Tennessee Valley Authority Kingston Fossil Plant Harriman, Roane County, Tennessee	**Perimeter Containment** **North Dredge Cell (Dike C) Segment 1** **Sta. A161+50 to A179+50**
Document Control Number RDP-0113-E *Calculation Package* FPGKIFFESCDX00030020100006	

Exhibit 12
Liquefaction Above the Phreatic Surface

Purpose:

- Quantify the height of compacted ash above the phreatic surface within the closed landfill that is subject to liquefaction in the design earthquake.

Methods:

- Input information includes prediction of saturation profile above the phreatic surface, soil-water characteristic curves for Kingston ash, cyclic resistance ratios for the saturated ash, cyclic stress ratios for design earthquake
- The increased liquefaction resistance of the ash above the phreatic surface was estimated using empirical methods published by Okamura and Soga (2006) and Okamura and Noguchi (2009).

Results:

- Analyses suggest that 8 feet of landfilled ash above the phreatic surface should be expected to liquefy in the design earthquake.
- Results can be used to determine the needed vertical extents of the capillary break layer.

Calculation Performed by: Stantec Consulting Services, Inc.	
Prepared by: AFR 12-13-10	*Reviewed by:* YW 12-14-10
Revisions:	

Kingston Dredge Cell Closure Project
Liquefaction above the Phreatic Surface

1. Objective

The analyses documented here were undertaken to quantify how much of the compacted ash above the long-term phreatic surface (groundwater table) will liquefy in the design earthquake. In the post-earthquake stability analyses, unsaturated ash in this zone will be assigned residual strength parameters. The results will also be used in future design packages to help determine the needed extents of the capillary break layer within the closed Kingston dredge cell.

2. Introduction

Recovered ash will be placed in the dredge cell at a controlled water content; over time, however, the water content of this material is expected to gradually increase. The closed dredge cell will be capped with an engineered cover to limit the infiltration of surface water, but the deeper compacted ash will be subject to capillary rise of water from the groundwater table. Under the outslopes of the ash landfill, capillary rise will be controlled by the inclusion of a capillary break layer (coarse stone). The long-term, vertical profile of equilibrium moisture conditions above the phreatic surface were predicted, as described in Exhibit 6, for areas within the facility where a capillary break is not constructed. The water content of the compacted ash is expected to decrease with height above the phreatic surface.

Ash below the phreatic surface will be saturated and subject to liquefaction in the design earthquake. At short heights above the groundwater table, in the absence of a capillary break layer, the ash will become nearly saturated due to capillary rise and could liquefy. At higher elevations, the moisture content is expected to decrease significantly; air in the pores of the unsaturated ash will be highly compressible, while surface tension effects (arising from the air-water interfaces) will stiffen the material. For these reasons, unsaturated ash at elevations above some height over the groundwater table is not expected to liquefy in the design earthquake.

In geotechnical earthquake engineering, the usual practice is to consider the potential for liquefaction only in saturated soils below the groundwater table. There is a general understanding that liquefaction resistance increases rapidly with decreasing saturation above the phreatic surface. Liquefaction assessments are typically focused on sandy, natural soils, where the height of capillary rise is small to moderate due to the size of the pore spaces. In these soils, the thickness of potentially liquefiable material above the water table (where the saturation may be close to 100%) is limited and can be ignored.

For the Kingston project, the liquefiable material is a fine-grained ash. The material is susceptible to liquefaction, significant capillary rise, and greater retention of infiltrated water. Liquefaction to greater heights within the landfill during the design earthquake will place additional loads on the stabilized perimeter and reduce the stability of the landfill outslopes.

Hence, for this project, it is important to consider the potential for liquefaction of the unsaturated ash in the zone just above the long-term phreatic surface.

3. Approach for Analysis

To arrive at a prediction of liquefied thickness above the phreatic surface, a number of separate analyses must be completed:

1. Determine if the compacted ash will be contractive and susceptible to liquefaction.
2. Predict the long-term moisture profile in the unsaturated ash above the phreatic surface.
3. Use a soil-water characteristic curve to relate saturation levels with the matric suction in the ash.
4. Quantify the increase in liquefaction resistance in the unsaturated ash due to:
    a. increased compressibility of the pore fluid, and
    b. increased stiffness from the higher stress state.
5. Quantify the liquefaction resistance of the compacted ash, if saturated.
6. Predict the cyclic stresses in the ash generated by the design earthquake.
7. Compute the factor of safety above the phreatic surface and determine the liquefied thickness.

These analyses were completed as discussed in the succeeding sections of this Exhibit.

4. Contractive Behavior in Compacted Ash

The project will involve the compaction of ash in an embankment fill behind a stabilized perimeter. Groundwater will mound within the compacted ash over the long term, as predicted by the ground water model (Exhibit 5). Hence, the zone of interest for the current analysis is comprised of the compacted ash.

The compacted ash will not be susceptible to a liquefaction failure if, given the density and effective stress conditions, the material exhibits a dilative response. A relatively dense soil under a relatively low confining pressure will tend to expand when sheared, such that dilative soils do not experience liquefaction flow failures. Dilative soil states plot below the steady state line, which can be defined on a plot of effective stress and void ratio using data from drained or undrained laboratory tests.

The steady state line for the Kingston fly ash was determined by laboratory testing during the Root Cause investigation and is shown in Figure 1 (AECOM 2009). Note that the critical void ratio (from drained tests) and the steady state (from undrained tests) lines in Figure 1 should be more similar. AECOM (2009) indicates that the difference may be due to particle breakage and the re-use of samples for drained testing, and further recommend that the steady state line should be used. On average, the landfilled ash is expected to have a dry

unit weight of 87 pcf and a void ratio of 0.67 (Exhibit 3), which would be on the dilative side of the steady state line in Figure 1 for stresses less than 10,000 psf.

The unsaturated zone within the landfill will be 40 feet thick or less, with an average moist unit weight of 109 pcf, corresponding to a maximum effective stress of about 4,400 psf. The specifications for compaction of the ash require a density greater than 90% of the maximum density determined from a Proctor compaction test with standard energy. Based on the Proctor tests reported in Exhibit 3, the ash must be compacted to a dry unit weight of 75 pcf or higher (void ratio of 0.91 or lower). Anticipating that wet conditions during construction will, from time to time, make it difficult to achieve the desired compaction, it is prudent to assume that some strata within the landfill will be placed at the loosest allowable void ratio of 0.91.

The expected conditions above the phreatic surface within the closed landfill (effective stress up to 4,400 psf and void ratio less than 0.91) are superimposed on AECOM's plot in Figure 1. For the deeper, more loosely compacted ash near the phreatic surface, this plot indicates a significant potential range of conditions where the ash would be contractive. Hence, liquefaction within the compacted ash cannot be ruled out based on material density, and the design needs to consider the potential for liquefaction of the landfilled ash in the capillary zone just above the groundwater table.

5. Saturation Profile above the Phreatic Surface

The amount of water within the ash can be expressed using any one of three quantities.

- The degree of saturation (S_r) is the ratio (typically expressed as a percentage) of the volume of water (V_w) to the volume of voids (V_v) within the soil:

$$Degree\ of\ Saturation = S_r = \frac{V_w}{V_v} \qquad \text{Eq. 1}$$

- The volumetric water content (θ) is the ratio of the volume of water to the total volume (V_t) of the soil:

$$Voumetric\ Water\ Content = \theta = \frac{V_w}{V_t} \qquad \text{Eq. 2}$$

- The gravimetric water content (w) is the ratio of the weight of water (W_w) to the weight of the solids (W_s) within the soil:

$$Gravimetric\ Water\ Content = w = \frac{W_w}{W_s} \qquad \text{Eq. 3}$$

These quantities can be related to one another, given the void ratio (e) and the specific gravity of the solids (G_s):

$$\theta = \frac{S_r\, e}{1+e} = \frac{G_s\, \omega}{1+e} \qquad \text{Eq. 4}$$

For Kingston fly ash, G_s = 2.31 and an average void ratio of e = 0.67 is expected within the compacted embankment. This analysis for liquefaction will assume the more critical limiting case of e = 0.91, corresponding to the loosest density that would be allowed by the compaction specification.

Above the phreatic surface (groundwater table) in the closed landfill, the long-term moisture content of the compacted ash will vary with elevation. The water content is affected by

infiltration through the landfill cover, capillary rise from below, and the water retention characteristics of the ash.

The expected profile of moisture content was predicted by finite element analysis documented in Exhibit 6. The calculations were made using laboratory data from five separate samples of Kingston fly ash, and were reported in terms of volumetric water content and degree of saturation. Parametric analyses demonstrated that the results for the long-term conditions were not sensitive to the assumed initial water content.

The predicted profiles of saturation above the phreatic surface are re-plotted here in Figure 2. The conditions within about 10 feet of the phreatic surface are expected to be critical in the assessment for liquefaction. Hence, the higher saturation predicted from the Kingston sample “kif-5” data were carried forward in this analysis.

6. Soil-Water Characteristic Curve

The assessment of liquefaction potential for unsaturated soils requires quantifying the matric suction:

$$Matric\ Suction = (u_a - u_w) \qquad \text{Eq. 5}$$

where u_a is the pore air pressure and u_w is the pore water pressure in the soil. The matric suction can be related to the water content (or degree of saturation) using a soil-water characteristic curve for a particular soil, derived from laboratory tests.

Data relating matric suction to saturation for three Kingston ash samples were generated by laboratory testing reported by Daniel B. Stephens and Associates (1989). In that report, the “main drainage curves” represent wetting conditions in the ash, while “initial drainage curves” represent drying conditions. The data are plotted here in Figure 3. The expected behavior is for the wetting curve data to fall below (lower saturation at a given matric suction) the drying curve data. The results in Figure 3 do not follow this trend, and the wetting curve data appears questionable. Hence, the more conservative drying curve data (lower matric suction for a given saturation level) were used in this assessment. The void ratios of these three test specimens were in the range of 0.81 to 0.85, consistent with the densities assumed for this liquefaction analysis.

The three measured drying curves (soil-water characteristic curves) for the Kingston ash are plotted in Figure 4. A conservative application of this data is represented by the lower bound of this data. For the liquefaction assessment, the lower bound soil-water characteristic curve was represented by the multilinear curve in Figure 4 and defined by these equations:

$$100 \geq S_r > 90: \quad \log(u_a - u_w) = (100 - S_r)/4 \qquad \text{Eq. 6}$$

$$90 \geq S_r > 79: \quad \log(u_a - u_w) = (140 - S_r)/20 \qquad \text{Eq. 7}$$

$$79 \geq S_r > 35: \quad \log(u_a - u_w) = (323 - S_r)/80 \qquad \text{Eq. 8}$$

where S_r is the degree of saturation in percent. Note that these equations are simple, multiple lines fit to the data for the convenience of the spreadsheet calculations (Appendix A), and do not represent fundamental relationships for the behavior of ash.

7. Increased Liquefaction Resistance of Unsaturated Ash

7.1. CRR of Unsaturated Soil

The great majority of liquefaction research has focused on the behavior of saturated soils, as there is a general understanding that unsaturated soils are much more resistant to liquefaction. De-saturating a soil deposit, perhaps by the injection of air, has been recognized as a potential means of mitigating liquefaction risks. Okamura and Soga (2006) point out that two mechanisms contribute to the increased liquefaction resistance in unsaturated soils:

(1) Air in the voids or pore space of the soil is highly compressible, such that volumetric contraction within an unsaturated soil can be absorbed by the compressible mix of pore air and water.

(2) Air in the pore voids creates surface tension effects, characterized with the matric suction, which increases the stiffness and strength of an unsaturated soil.

Recent laboratory research in Japan (Okamura and Soga 2006, Okamura and Noguchi 2009) has lead to a practical means of estimating the liquefaction resistance of unsaturated silt. Based on data from cyclic triaxial tests on unsaturated soils under controlled conditions, these authors developed empirical adjustment factors that quantify the added liquefaction resistance. Using different symbols than used in these publications, the Okamura methodology can be expressed as:

$$CRR_{unsat} = CRR_{sat} \cdot F_{comp} \cdot F_{suction} \qquad \text{Eq. 9}$$

where:

CRR_{unsat} = Cyclic Resistance Ratio for the unsaturated soil

CRR_{sat} = Cyclic Resistance Ratio for the same soil if saturated at the same void ratio

F_{comp} = empirical factor accounting for increased liquefaction resistance due to the increased compressibility of the pore fluid in the unsaturated soil (at low matric suction), as detailed in Section 7.2

$F_{suction}$ = empirical factor accounting for increased liquefaction resistance due to the increased soil stiffness from the matric suction in the unsaturated soil, as detailed in Section 7.3

7.2. Factor for Pore Fluid Compressibility

Okamura and Soga (2006) conducted laboratory tests on several sands using a special triaxial set-up where the pore water behaved as a compressible fluid, but without creating significant matric suction. This data was used to develop an empirical relationship for the "liquefaction resistance ratio" (LRR, identified here as F_{comp}). The correlation is shown in Figure 5. Okamura and Noguchi (2009) conducted additional tests on a silt material, and found the same empirical relationship worked well for that tested soil.

The compressibility factor can be computed as:

$$F_{comp} = \log_{10}(6500 \cdot \epsilon_v^* + 10) \quad \text{Eq. 10}$$

where ε^*_v is the potential volumetric strain defined below. The data supporting this correlation, plotted in Figure 5, extends only to values of $\varepsilon^*_v \leq 0.045$. Hence a maximum value of $F_{comp} = 2.5$ is assumed in the application of Equation 10.

The potential volumetric strain (ε^*_v) is derived from considerations for the compressibility of the pore fluid and Boyle's law (Okamura and Soga 2006). Using gage pressures, Okamura and Noguchi (2009) expressed ε^*_v as:

$$\epsilon_v^* = \frac{\sigma_c - u_{ao}}{\sigma_c + P_a}(1 - S_r)\frac{e}{1+e} \quad \text{Eq. 11}$$

where σ_c is the isotropic confining pressure, u_{ao} is the initial pore air pressure, P_a is one standard atmosphere of pressure, S_r is the degree of saturation, and e is the void ratio. In the field, the initial pore air pressure will be close to the atmospheric pressure (essentially zero gage pressure). The total confining pressure is anisotropic, but can be approximated with the total vertical stress (σ_v). Hence, Equation 11 can be written in this form for the application to field conditions:

$$\epsilon_v^* = \frac{\sigma_v}{\sigma_v + P_a}(1 - S_r)\frac{e}{1+e} \quad \text{Eq. 12}$$

This relationship is valid only for relatively high soil saturation. As indicated above, Okamura and Soga (2006) and Okamura and Noguchi (2009) show data only for values of $\varepsilon^*_v \leq 0.045$.

One could expect markedly different behavior at very low saturations (higher values of ε^*_v), where the pore water is found in pockets within the pore spaces. Plotting values of ε^*_v from Equation 12 as a function of S_r for the Kingston dredge cell, ε^*_v is observed to peak at a value of about 0.1 at a saturation of about 47%. This is well past the validated limit of ε^*_v = 0.045, corresponding to the assumed, maximum value of $F_{comp} = 2.5$.

7.3. Factor for Matric Suction

Okamura and Noguchi (2009) conducted cyclic tests on an unsaturated silt, and quantified the increase in liquefaction resistance compared to the same soil when saturated. Based on the previously defined compressibility factor (F_{comp}), they could attribute the increased strength separately to the effects of compressibility and matric suction. Hence, the definition of $F_{suction}$ below requires the concurrent application of F_{comp} from Equation 10.

Based on the work of Okamura and Noguchi (2009), the matric suction factor ($F_{suction}$) is defined by:

$$F_{suction} = \frac{\sigma_{net} + (u_a - u_w)(A_1 - 1)}{\sigma_c - u_{wo}} \quad \text{Eq. 13}$$

where σ_{net} is the net stress (total stress minus the pore air pressure), u_a is the pore air pressure, u_w is the pore water pressure, u_{wo} is the initial pore water pressure, σ_c is the isotropic confining pressure in the triaxial test, and A_1 is an empirical coefficient.

Okamura and Noguchi (2009) reported A_1 = 1.29 for the one soil they tested, and cautioned that this value may be not applicable to other soils or other densities. The soil they tested was a non-plastic silt comprised primarily of silica, with 100% of the particles finer than No. 200 sieve and a mean grain size of 0.012 mm. About 25% of the material was finer than

0.005 mm, but there was no clay mineral. The test specimens were compacted to a void ratio of 0.96. While different, the silt tested by Okamura and Noguchi (2009) appears to be a reasonable analogy for the compacted fly ash in the Kingston dredge cell.

In the field, the pore air pressure within the ash will be close to atmospheric pressure (zero gage pressure). The total confining pressure will be anisotropic, but can be approximated with the total vertical stress (σ_v). Then, for application to field conditions, Equation 13 can expressed as:

$$F_{suction} = \frac{\sigma_v + (u_a - u_w)(A_1 - 1)}{\sigma_v - u_{wo}} \qquad \text{Eq. 14}$$

A value of A_1 = 1.29 was assumed for the compacted fly ash.

8. Liquefaction Resistance in Saturated Ash

To quantify the liquefaction resistance of an unsaturated soil with Equation 9, the liquefaction resistance (cyclic resistance ratio, CRR_{sat}) must be estimated for the soil in a saturated state at the same void ratio. CRR_{sat} can be measured by cyclic laboratory testing or with in situ penetration data, using the methods outlined in Exhibit 11. However, penetration data is not available for the compacted ash in the future landfill. Here, the value of CRR_{sat} was estimated based on the penetration resistance (SPT blowcounts) measured in the sluiced ash deposits at the site.

Data from the AECOM borings within the dredge cell (100-, 300-, and 500-series borings) were used in this calculation. In the analysis, the depth of the SPT blowcount below the ground surface was assumed to be the same during the earthquake as the depth from the boring log. For example, a future blowcount in the landfilled ash 20 feet below the final cover was assumed to be the same as a blowcount measured 20 feet below the surface of the failed ash at the time of the boring. Within the ash, no fines content corrections were applied. The water table was assumed to be 30 feet below the surface at the time of the earthquake, consistent with the predicted conditions for the closed landfill (Exhibit 5). The capillary break will extend under the outslopes, so this assessment is focused on areas under the relatively flat central cover, where the surface slope will be 2% or less. Hence, the static shear stress factor (K_α) was assumed to be one. From the ground response analyses (Exhibit 10), the local earthquake event will be more critical for liquefaction within the landfilled ash, so the magnitude scaling factor was computed for M_w = 6.0.

The results of this analysis are plotted in Figure 6. There are a substantial number of data points near the lower bound of CRR_{sat} = 0.07, corresponding to locations where low blowcounts were measured.

A value of CRR_{sat} = 0.07 was thus selected to represent the compacted ash in the capillary fringe within the landfill. This estimate should be appropriate, because the sluiced ash deposits had an average void ratio of 0.85, while the compaction specification (requiring a density no less than 90% of the standard Proctor maximum) will result in ash void ratios of 0.91 or less.

9. Cyclic Stress from the Design Earthquake

One-dimensional ground response analyses were carried out following the methods described in Exhibit 10. Assuming a ground surface elevation of 790 feet, input ground motion time histories for the M_w = 6.0 local event were applied to the landfill using SHAKE. The predicted maximum shear stresses increase with depth below the ground surface. To facilitate subsequent computations, a fourth-order polynomial was fit to the results:

$$\tau_{max} = -1.81x10^{-5}\, z^4 + 0.00457\, z^3 - \ 0.4748\, z^2 + \ 26.58\, z \qquad \text{Eq. 15}$$

where τ_{max} is the maximum induced shear stress (psf) and z is the depth (feet) below the ground surface. The cyclic stress ratio (CSR) can then be computed at any depth as:

$$CSR = 0.65\ \frac{\tau_{max}}{\sigma'_v} \qquad \text{Eq. 16}$$

The resulting values within the landfilled ash are plotted in Figure 7.

10. Results

Calculations for the evaluation of liquefaction above the phreatic surface were accomplished using the spreadsheet provided in Appendix A. The liquefaction calculations conservatively assume a void ratio of 0.91 in the ash, corresponding to the loosest density that would be allowed by the compaction specification.

The water content (volumetric and gravimetric) and degree of saturation were obtained from finite element predictions (Exhibit 6) based on the properties of the “kif-5” sample from Figure 2. These moisture profiles are plotted here in Figure 8. The matric suction was then computed from Equations 6 through 8, corresponding to the lower-bound soil-water characteristic curve in Figure 4. This then allowed the calculation of the stress profiles plotted in Figure 9.

The potential volumetric strain (Figure 10) was computed using Equation 12. The liquefaction resistance factors for unsaturated soils, F_{comp} and $F_{suction}$, were then computed using Equations 10 and 14, respectively. The resulting values are plotted in Figure 11. Finally, using a cyclic resistance ratio of CRR_{sat} = 0.07 for the ash in a saturated condition, the liquefaction resistance of the unsaturated ash (CRR_{unsat}) could be computed using Equation 9. These results are plotted in Figure 12, together with the cyclic stress ratio computed using Equations 15 and 16.

The factor of safety against liquefaction in the unsaturated ash can then be computed as:

$$FS_{liq} = \frac{CRR_{unsat}}{CSR} \qquad \text{Eq. 17}$$

The resulting values are plotted against height above the phreatic surface in Figure 13. Given the limited experimental data that supports the definitions of F_{comp} and $F_{suction}$, all of the ash in the capillary zone with $FS_{liq} \leq 1.4$ is judged to liquefy in the design earthquake. From the results given in Appendix A and plotted in Figure 13, the ash within 7.5 feet above the phreatic surface is thus expected to liquefy. Within this zone, the ash is expected to have a saturation greater than about 97%. For a void ratio of 0.91, this corresponds to a gravimetric water content greater than about 38%.

Note that the calculations presented here are not considered reliable for the higher elevations within the closed ash landfill. There is insufficient data to define F_{comp} values greater than 2.5, for ε^*_v greater than about 0.045. For the conditions within compacted ash in the closed dredge cell, this computational limit occurs at a height of about 13.5 above the phreatic surface.

11. Conclusion

The recovered ash to be placed in the landfill will be compacted, but the compaction specifications will allow a dry density that is 90% of the standard Proctor maximum. At this somewhat loose density and under the expected stress conditions, a significant portion of the saturated ash will likely be contractive and subject to liquefaction in the design earthquake event.

In the unsaturated ash beneath the landfill cover, and in areas above the capillary break, the degree of saturation in the ash will be low. With significant air in the pores of the ash, the high compressibility of the pore fluid (air and water), coupled with the increased stiffness due to surface tension, should be more than sufficient to prevent liquefaction within the landfilled ash.

Nearer the long-term water table, the ash will be almost saturated due to capillary rise. Hence, within some distance above the groundwater table, the ash is subject to liquefaction. The analyses presented in this section, which rely upon recently published laboratory research, indicate that about 7.5 feet of ash above the phreatic surface will liquefy in the design earthquake at this site. This zone corresponds to the height of ash where the degree of saturation exceeds 97%.

For the project design, ash within 8 feet above the phreatic surface will be assumed to liquefy in the design earthquake event. At greater heights above the phreatic surface, the ash is predicted to not liquefy.

12. References

AECOM (2009). “Root Cause Analysis of TVA Kingston Dredge Pond Failure on December 22, 2008.” Four volumes, June 25.

Daniel B. Stephens and Associates, Inc. (1989). “Laboratory Analysis of Hydraulic Properties of Kingston and Colbert Fly Ash.” Prepared for TVA, August.

Okamura, M., and Noguchi, K. (2009). “Liquefaction Resistances of Unsaturated Non-Plastic Silt.” *Soils and Foundations, Japanese Geotechnical Society.* Vol. 49, No. 2, April, pp. 221-229.

Okamura, M., and Soga, Y. (2006). “Effects of Pore Fluid Compressibility on Liquefaction Resistance of Partially Saturated Sand.” *Soils and Foundations, Japanese Geotechnical Society.* Vol. 46, No. 5, October, pp. 695-700.

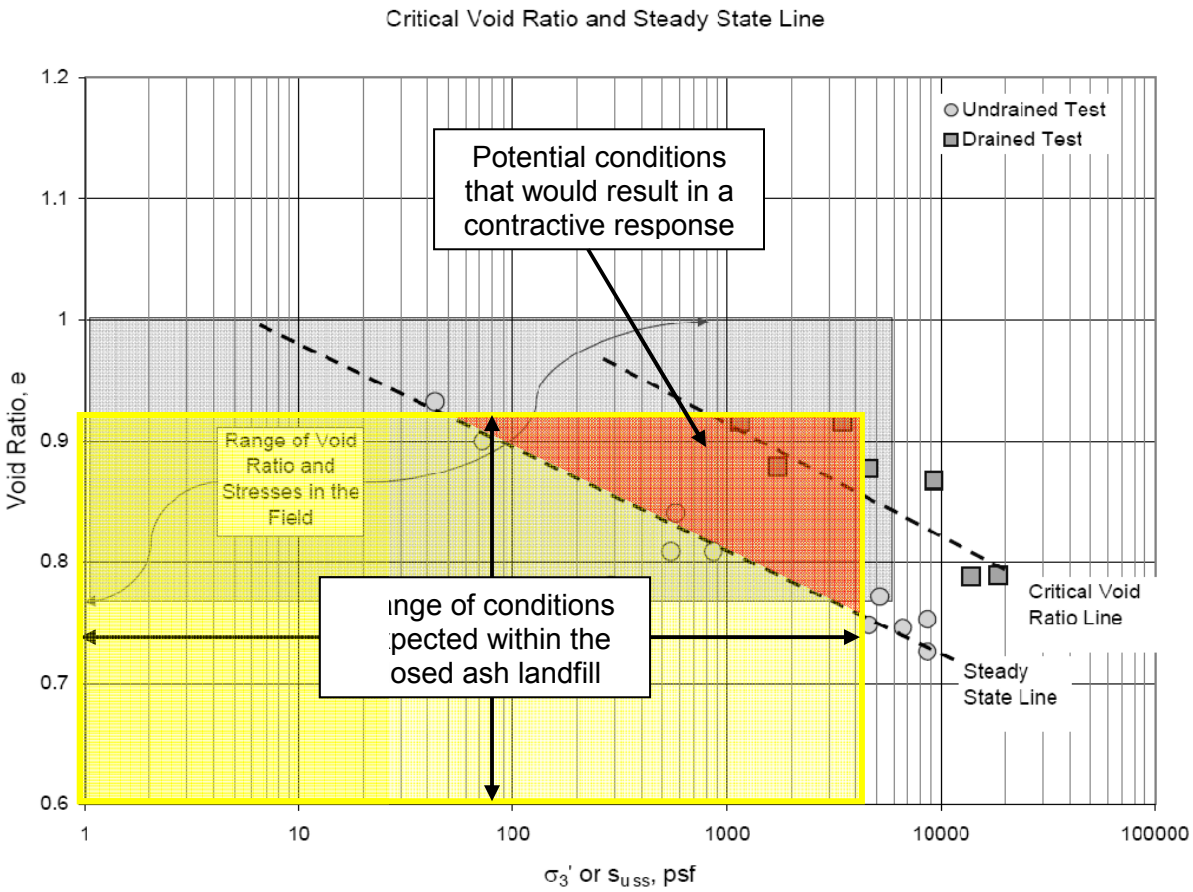

Figure 1. Steady state line for Kingston fly ash (from AECOM 2009) with expected range of void ratio and effective stresses within the compacted ash landfill.

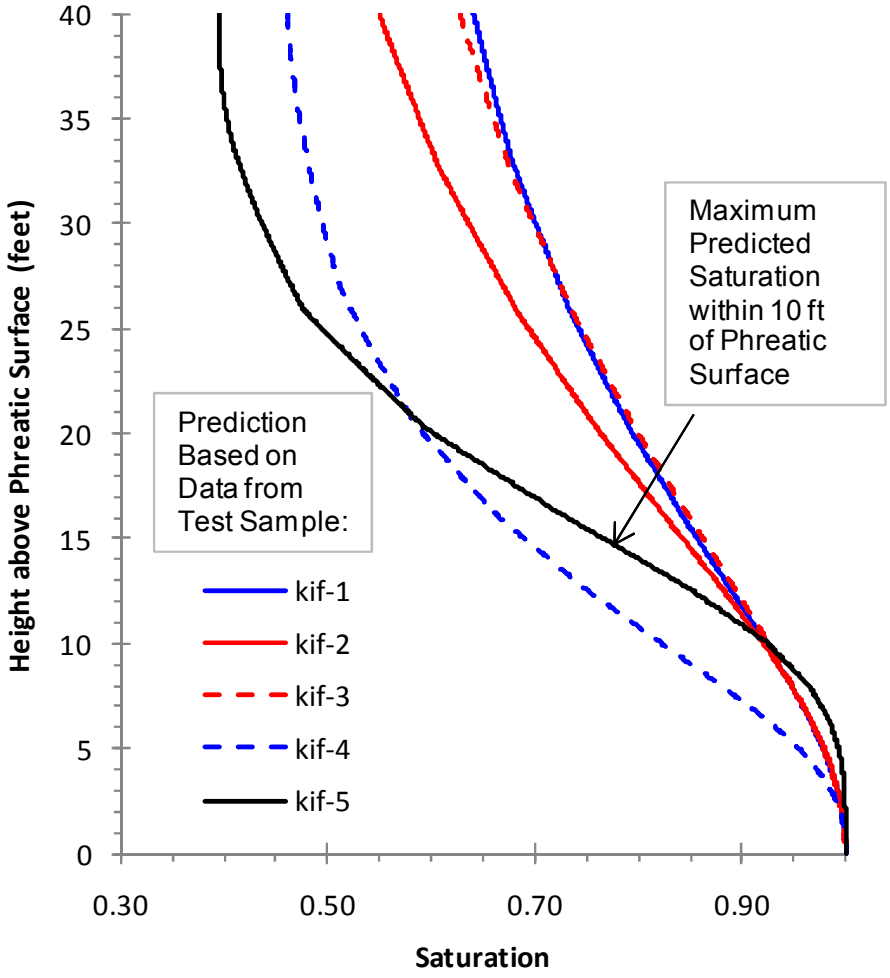

Figure 2. Profiles of predicted saturation above the groundwater table in the closed landfill, based on finite element analyses (see Exhibit 6).

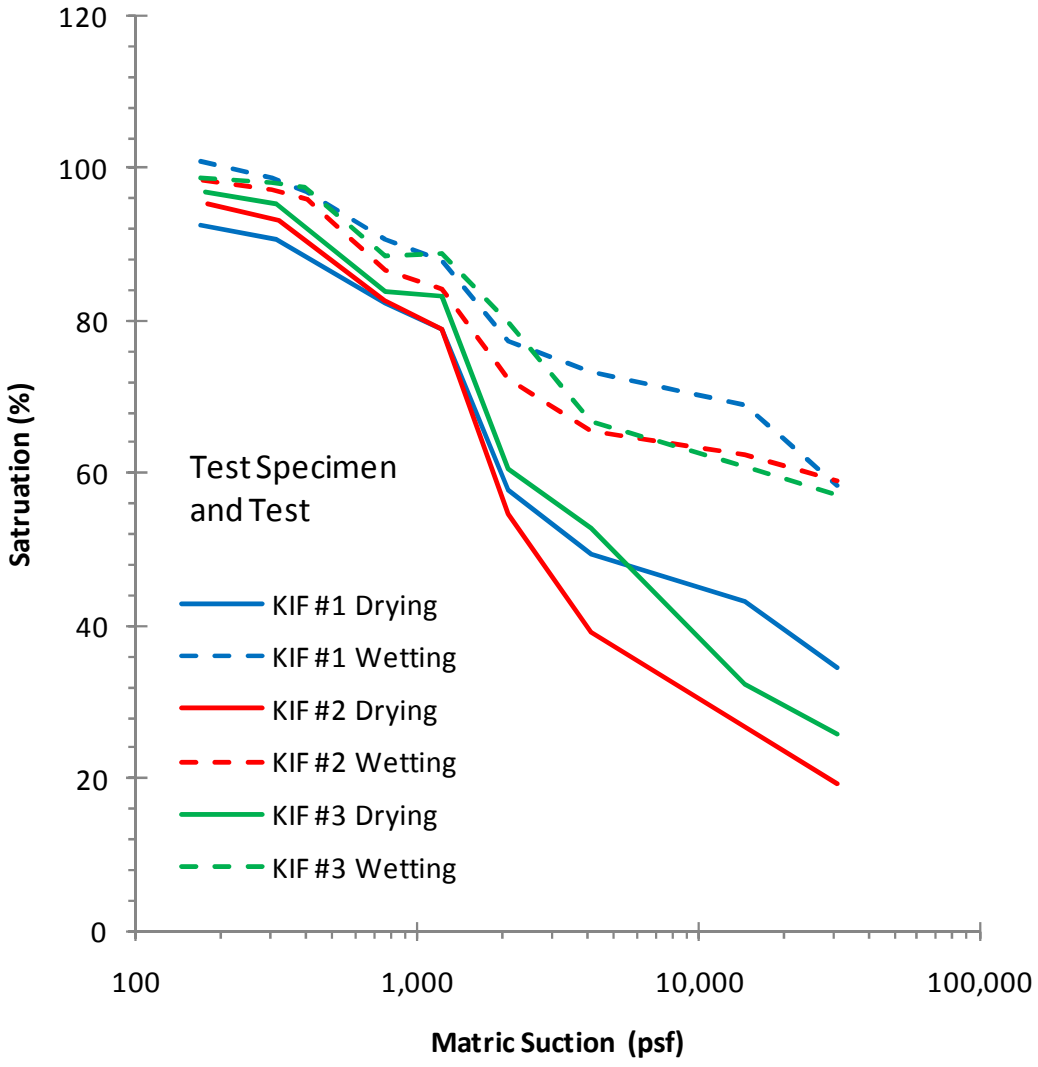

Figure 3. Soil-water characteristic curves for three samples of Kingston fly ash (data from D. B. Stephens and Associates 1989).

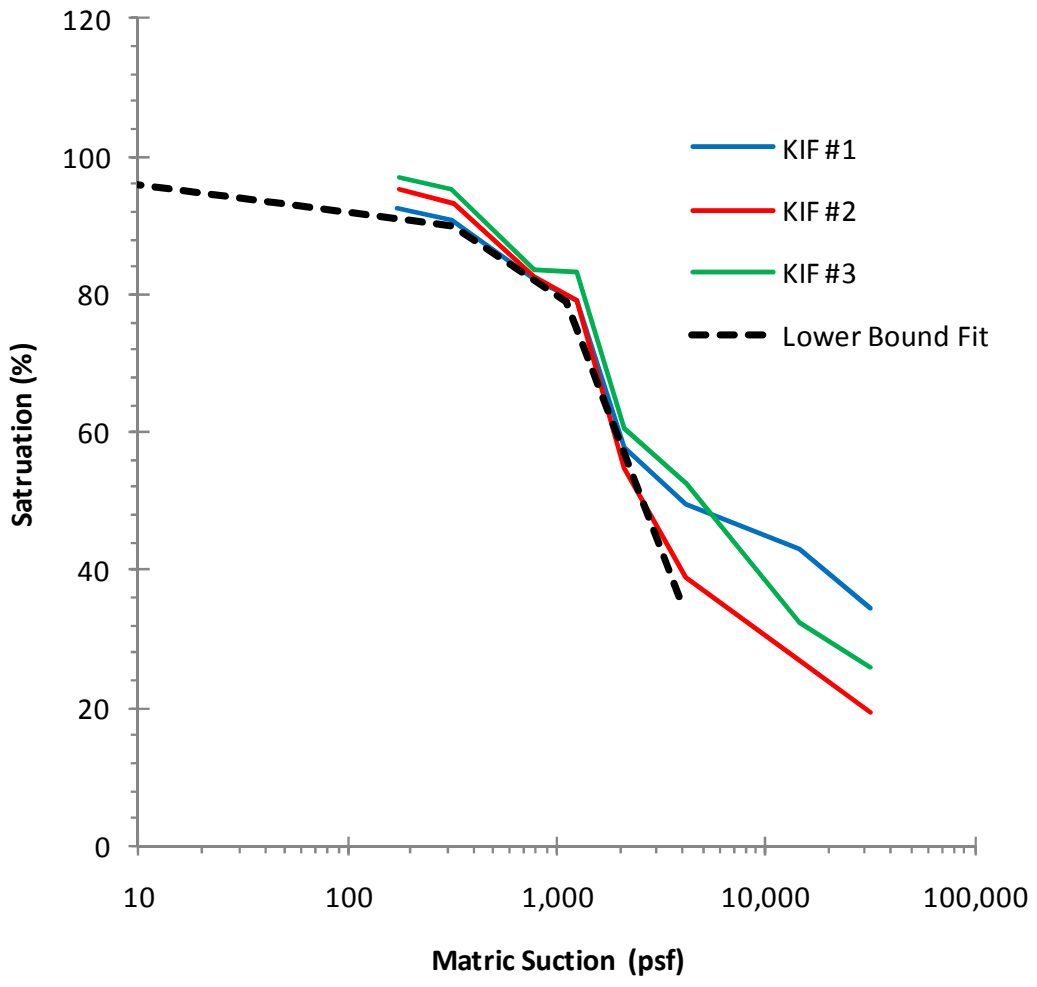

Figure 4. Soil-water characteristic curves used in the liquefaction assessment.

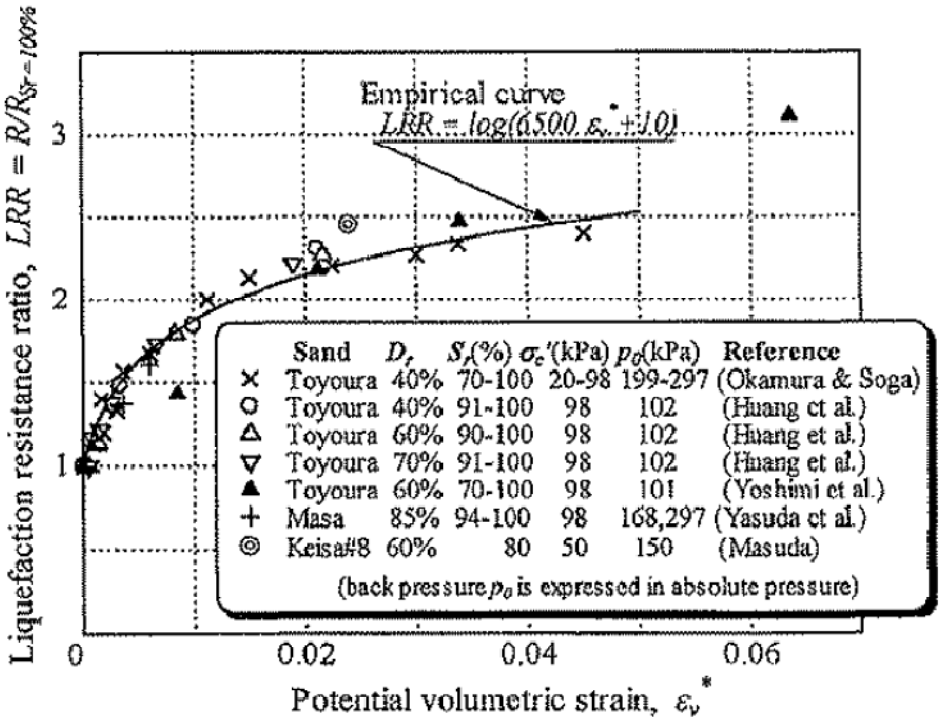

Figure 5. Empirical relationship for compressibility factor, F_{comp} = LRR (from Okamura and Noguchi 2009).

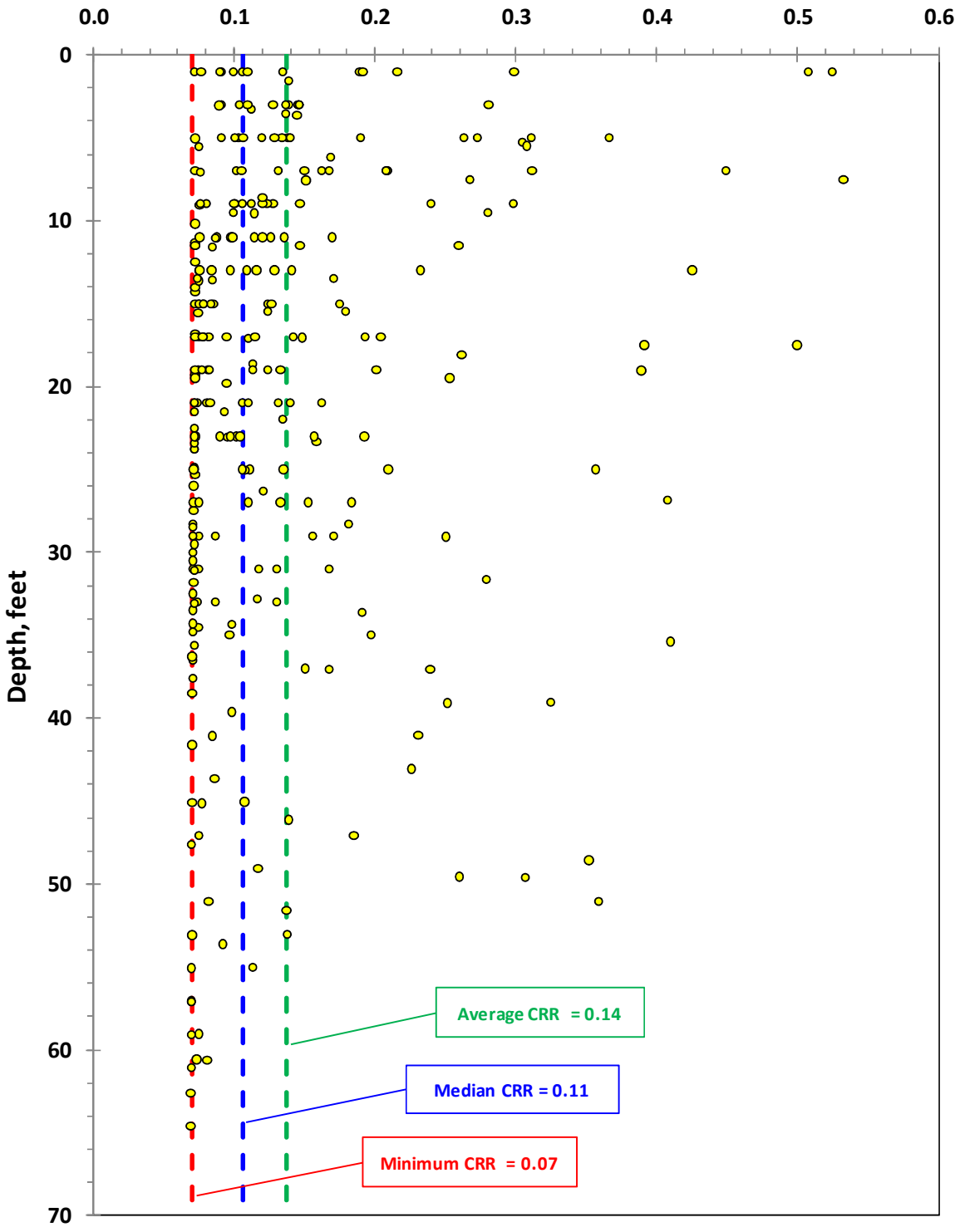

Figure 6. Cyclic resistance ratio in saturated ash (CRR_{sat}), computed using SPT data from AECOM borings in the 100-, 300-, and 500-series.

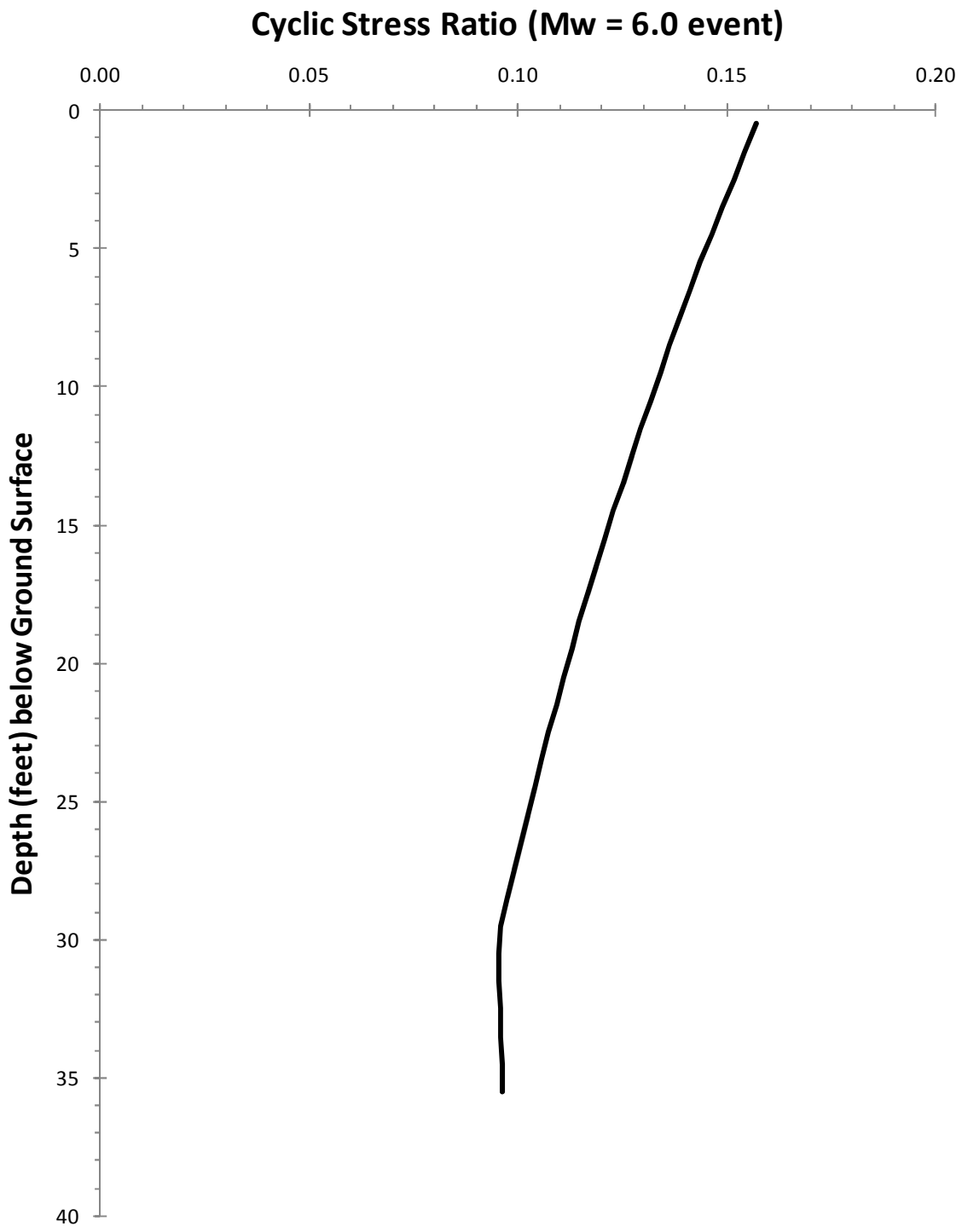

Figure 7. Cyclic stress ratio predicted within the landfilled ash for the M_w = 6.0 design earthquake event.

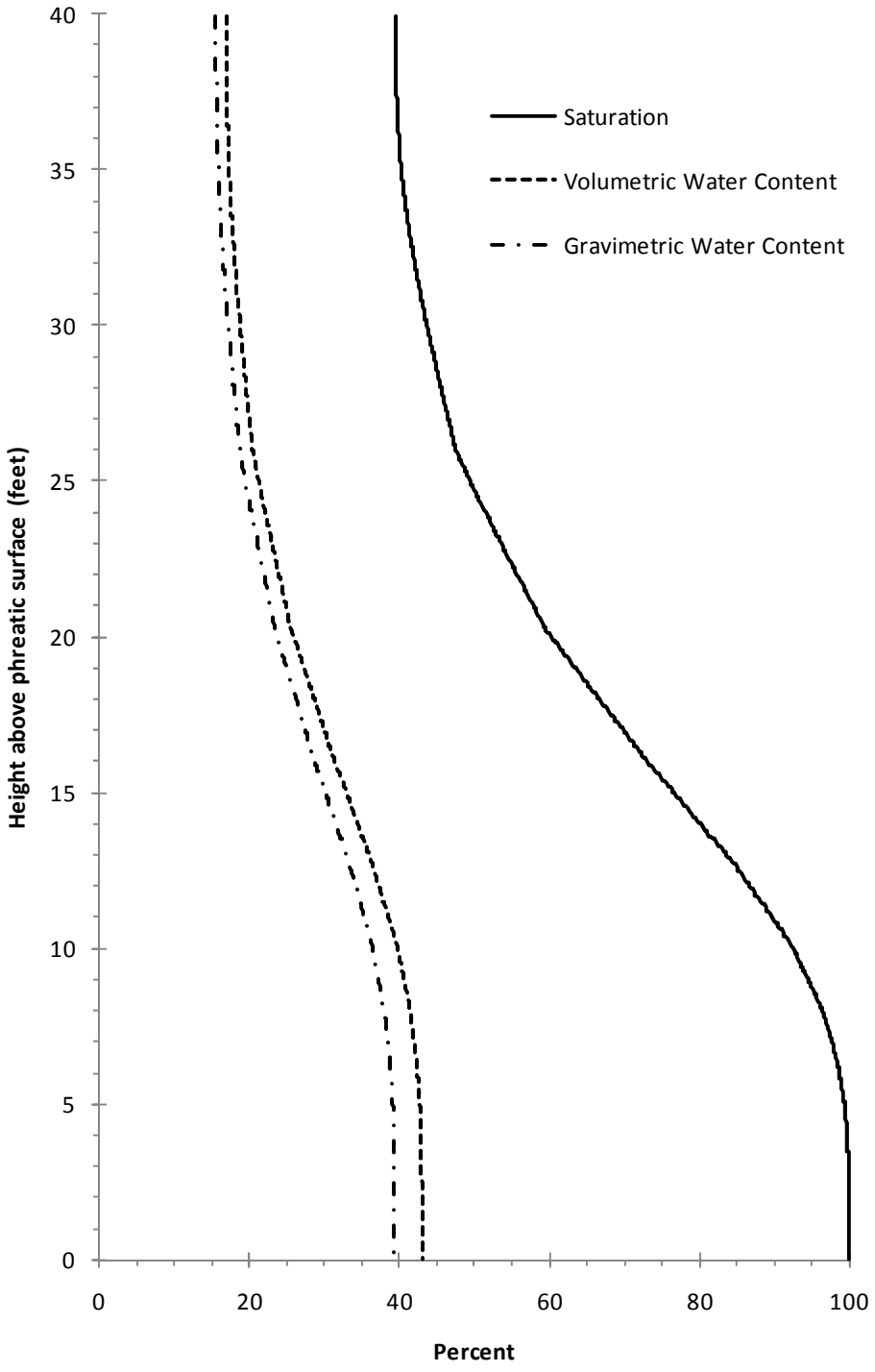

Figure 8. Predicted saturation and water content of ash above the phreatic surface.

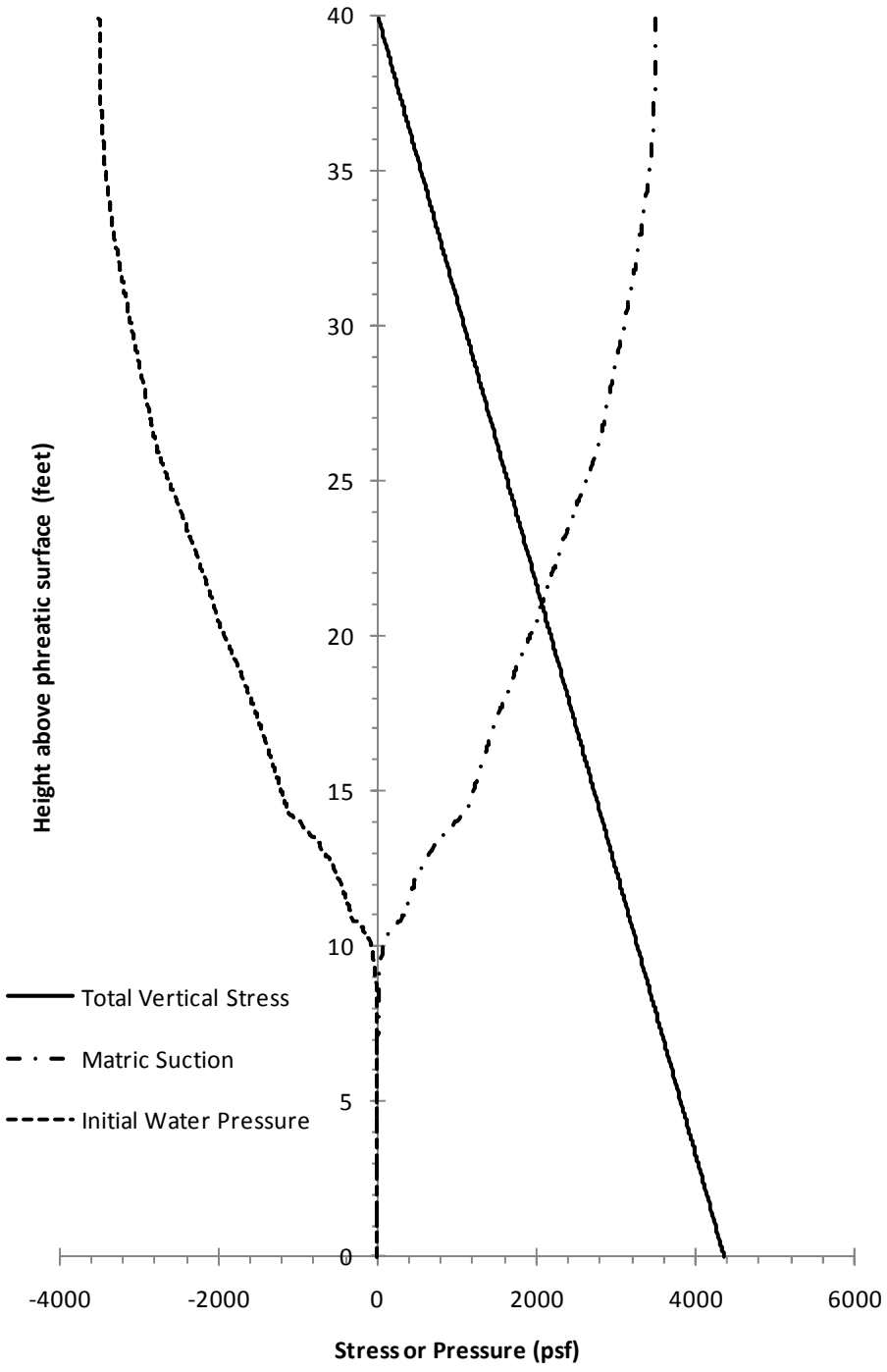

Figure 9. Predicted, long-term stress conditions within the ash above the phreatic surface.

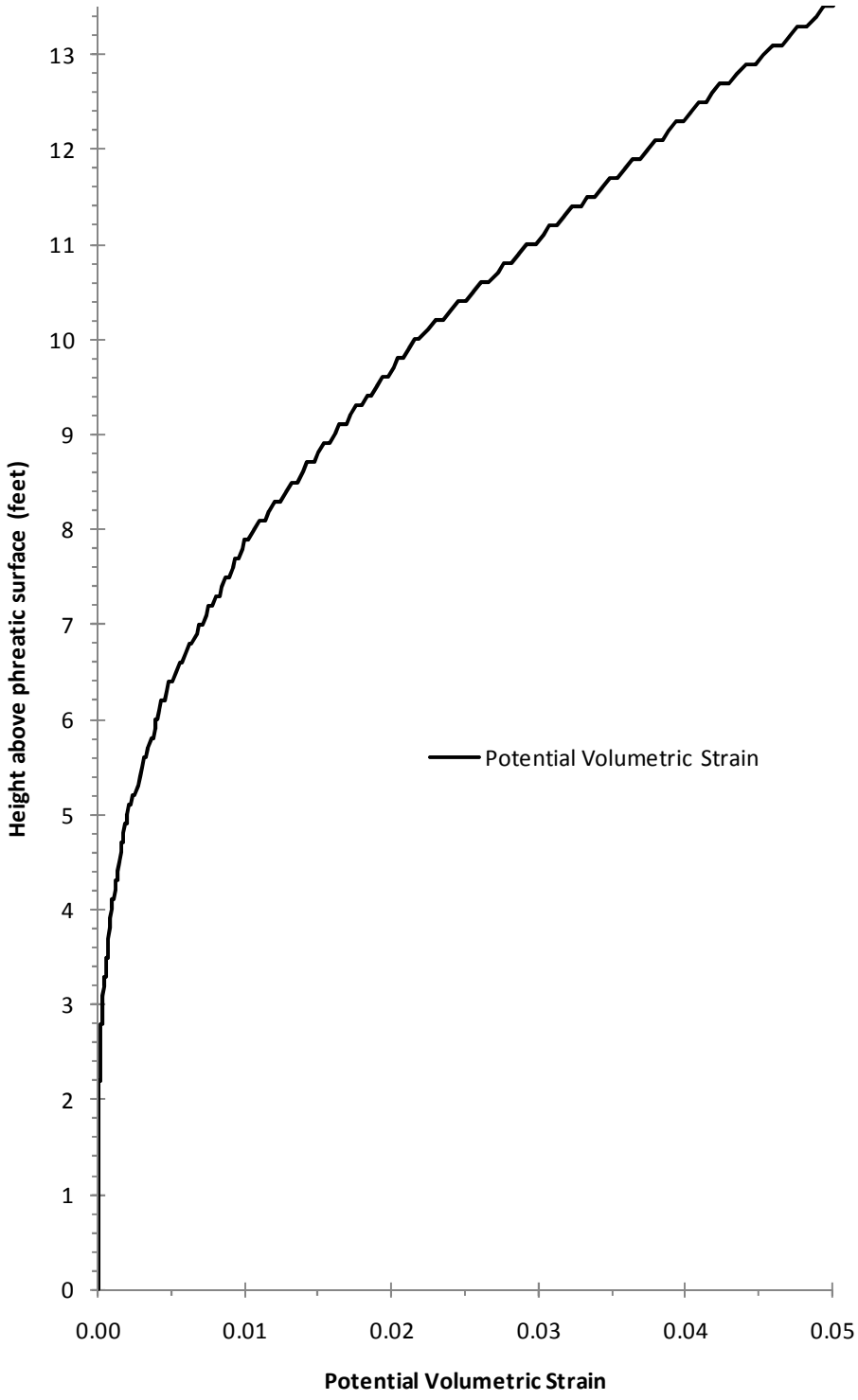

Figure 10. Predicted potential volumetric strain (ε^*_v , Equation 12) in the ash above the phreatic surface.

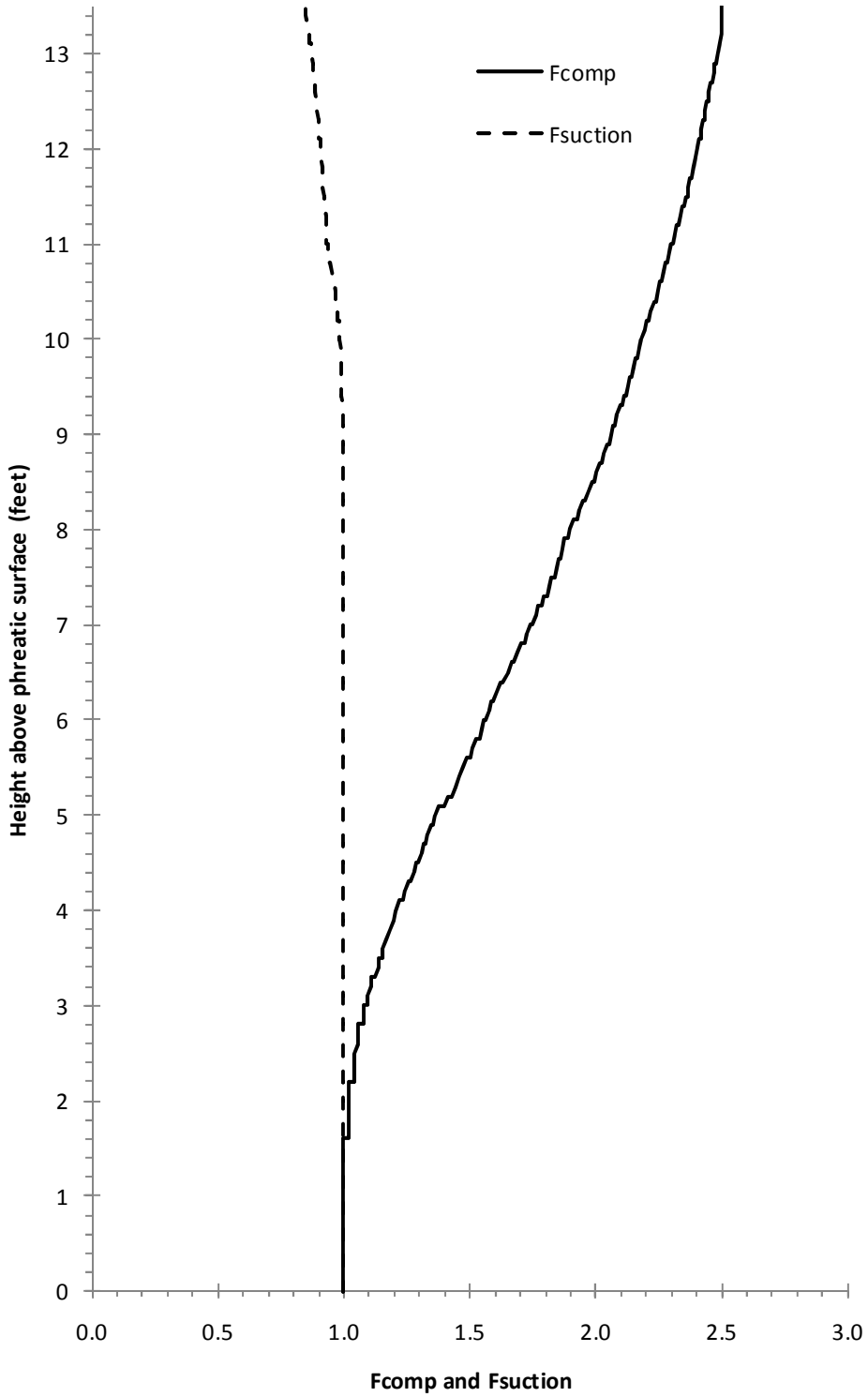

Figure 11. Factors for estimating the liquefaction resistance of the unsaturated ash above the phreatic surface, computed using Equations 10 and 14.

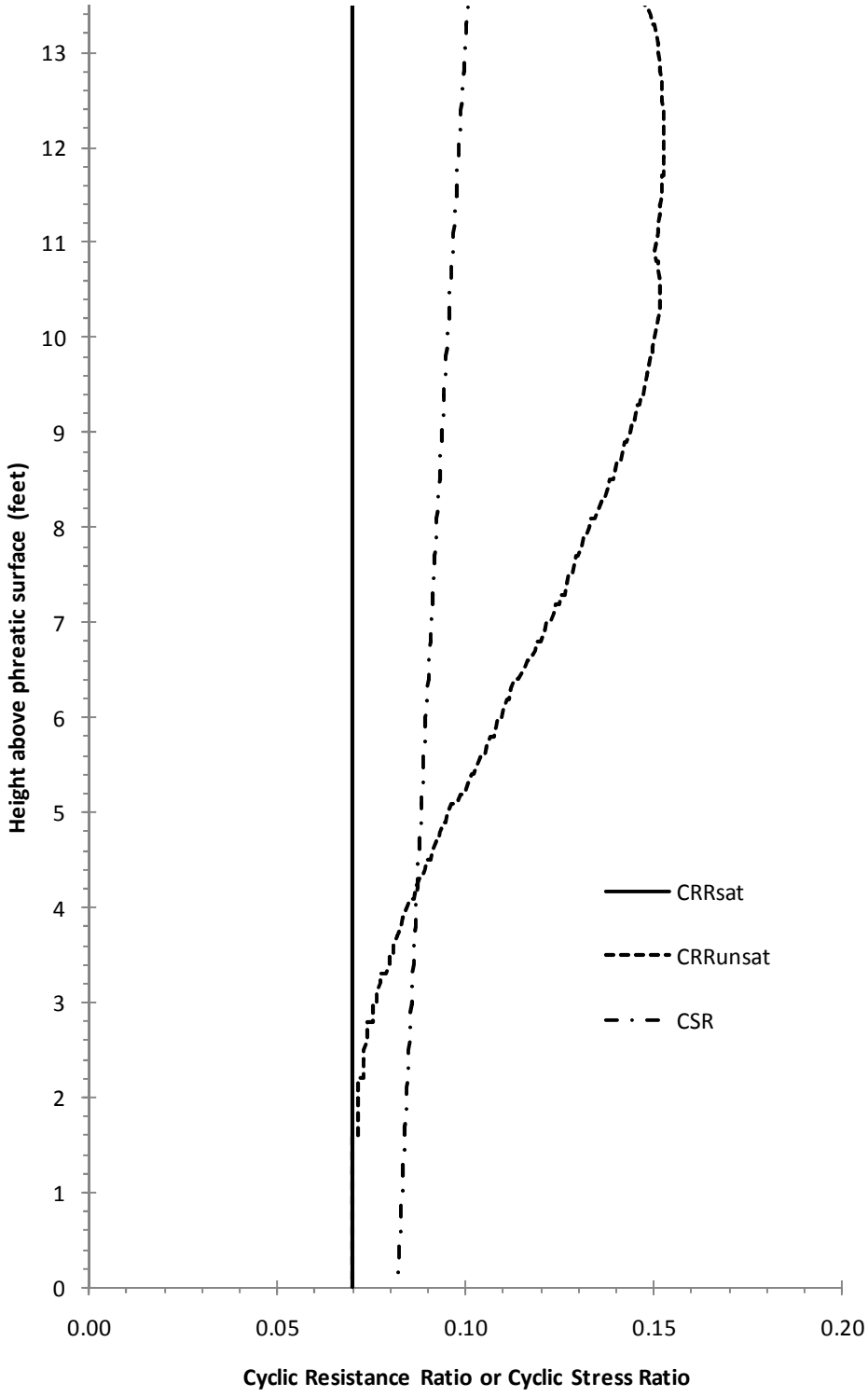

Figure 12. Cyclic resistance ratios and cyclic stress ratio computed in the ash above the phreatic surface.

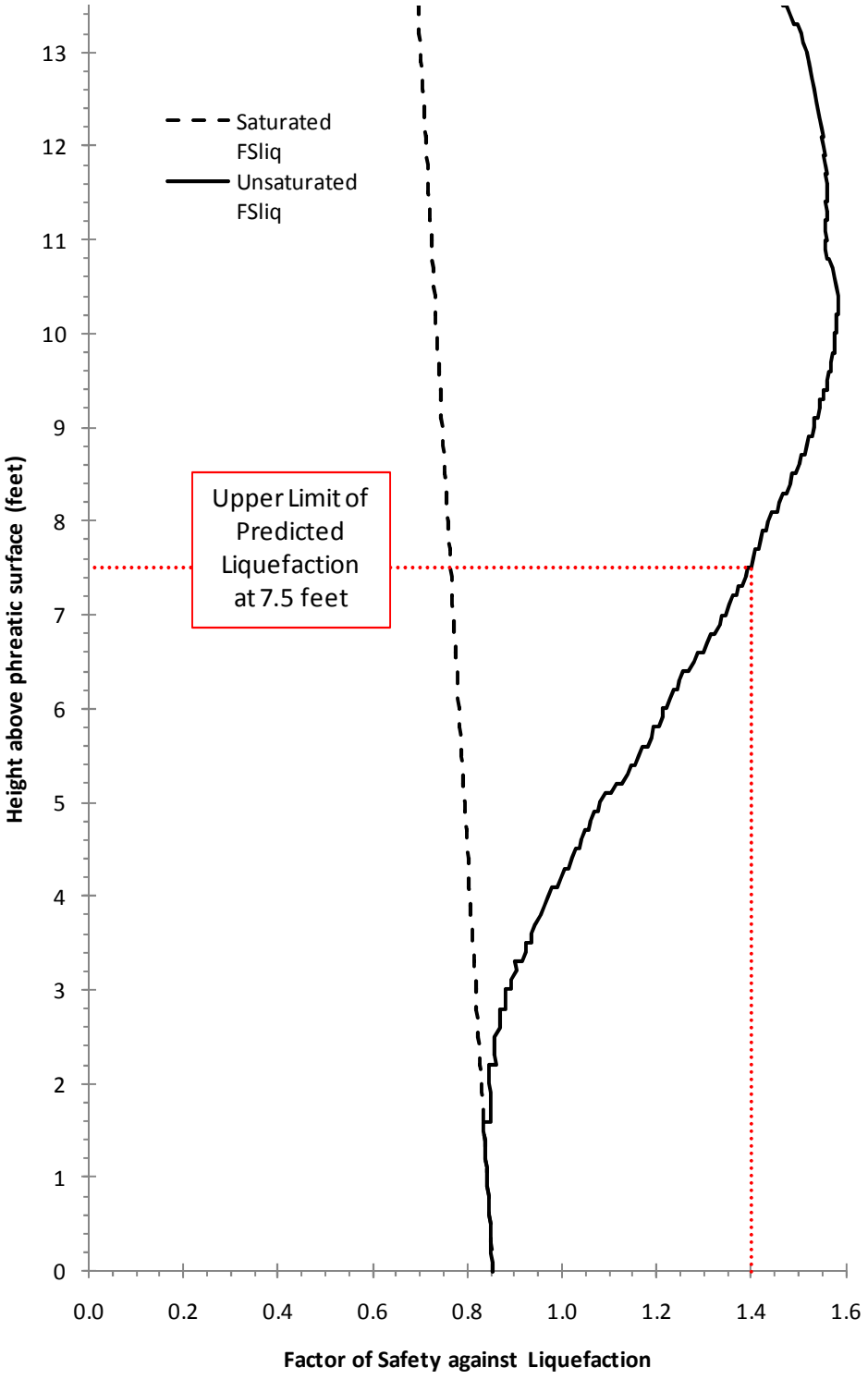

Figure 13. Factor of safety against liquefaction computed for the ash above the phreatic surface in the closed Kingston dredge cell.

Appendix A

Calculation Spreadsheets

Kingston Closure Project
Analysis for Liquefaction in the Capillary Fringe

Atmospheric Pressure	2116 psf		Moist Unit Weight of Compacted Ash	109 pcf
Unit Weight of Water	62.4 pcf		Void Ratio of Compacted Ash	0.91
Ground Surface Elevation	790 feet		Specific Gravity of Ash	2.31
Phreatic Surface Elevation	750 feet			

Height above Phreatic Surface feet	Depth below Ground Surface feet	Total Vertical Stress psf	Effective Vertical Stress psf	Volumetric Water Content %	Gravimetric Water Content %	Saturation %	Matric Suction psf	Initial Water Pressure psf	Potential Volumetric Strain	Fcomp	Fsuction	CRRsat	CRRunsat	Maximum Cyclic Shear Stress psf	CSR	Saturated FSliq	Unsaturated FSliq
13.5	26.5	2888.5	2888.5	35.2	32.2	81.8	813.7	-813.7	0.0501	2.500	0.844	0.07	0.15	447.1	0.101	0.70	1.47
13.5	26.5	2888.5	2888.5	35.3	32.3	82.0	792.2	-792.2	0.0494	2.500	0.847	0.07	0.15	447.1	0.101	0.70	1.47
13.4	26.6	2899.4	2899.4	35.4	32.4	82.3	771.3	-771.3	0.0489	2.500	0.851	0.07	0.15	448.1	0.100	0.70	1.48
13.3	26.7	2910.3	2910.3	35.5	32.5	82.5	750.9	-750.9	0.0483	2.500	0.854	0.07	0.15	449.0	0.100	0.70	1.49
13.3	26.7	2910.3	2910.3	35.6	32.6	82.7	731.1	-731.1	0.0477	2.500	0.857	0.07	0.15	449.0	0.100	0.70	1.50
13.2	26.8	2921.2	2921.2	35.7	32.7	83.0	711.7	-711.7	0.0471	2.500	0.861	0.07	0.15	450.0	0.100	0.70	1.50
13.1	26.9	2932.1	2932.1	35.8	32.8	83.2	692.9	-692.9	0.0465	2.495	0.864	0.07	0.15	450.9	0.100	0.70	1.51
13.1	26.9	2932.1	2932.1	35.9	32.9	83.4	674.6	-674.6	0.0459	2.489	0.867	0.07	0.15	450.9	0.100	0.70	1.51
13.0	27.0	2943.0	2943.0	36.0	33.0	83.7	656.8	-656.8	0.0453	2.484	0.870	0.07	0.15	451.9	0.100	0.70	1.52
12.9	27.1	2953.9	2953.9	36.1	33.0	83.9	639.5	-639.5	0.0447	2.478	0.874	0.07	0.15	452.9	0.100	0.70	1.52
12.9	27.1	2953.9	2953.9	36.2	33.1	84.1	622.6	-622.6	0.0441	2.472	0.876	0.07	0.15	452.9	0.100	0.70	1.52
12.8	27.2	2964.8	2964.8	36.3	33.2	84.3	606.1	-606.1	0.0435	2.467	0.879	0.07	0.15	453.8	0.099	0.70	1.53
12.7	27.3	2975.7	2975.7	36.4	33.3	84.6	590.1	-590.1	0.0429	2.461	0.883	0.07	0.15	454.7	0.099	0.70	1.53
12.7	27.3	2975.7	2975.7	36.5	33.4	84.8	576.1	-576.1	0.0423	2.455	0.885	0.07	0.15	454.7	0.099	0.70	1.53
12.6	27.4	2986.6	2986.6	36.6	33.5	85.0	562.3	-562.3	0.0418	2.450	0.887	0.07	0.15	455.7	0.099	0.71	1.53
12.5	27.5	2997.5	2997.5	36.6	33.6	85.2	550.4	-550.4	0.0414	2.445	0.890	0.07	0.15	456.6	0.099	0.71	1.54
12.5	27.5	2997.5	2997.5	36.7	33.6	85.4	538.8	-538.8	0.0409	2.440	0.892	0.07	0.15	456.6	0.099	0.71	1.54
12.4	27.6	3008.4	3008.4	36.8	33.7	85.6	527.3	-527.3	0.0404	2.435	0.894	0.07	0.15	457.5	0.099	0.71	1.54
12.3	27.7	3019.3	3019.3	36.9	33.8	85.7	516.2	-516.2	0.0399	2.431	0.896	0.07	0.15	458.5	0.099	0.71	1.55
12.3	27.7	3019.3	3019.3	37.0	33.9	86.0	503.9	-503.9	0.0393	2.424	0.898	0.07	0.15	458.5	0.099	0.71	1.54
12.2	27.8	3030.2	3030.2	37.0	33.9	86.1	493.2	-493.2	0.0389	2.420	0.901	0.07	0.15	459.4	0.099	0.71	1.55
12.1	27.9	3041.1	3041.1	37.1	34.0	86.3	482.7	-482.7	0.0384	2.415	0.903	0.07	0.15	460.3	0.098	0.71	1.55
12.1	27.9	3041.1	3041.1	37.2	34.1	86.5	472.5	-472.5	0.0379	2.409	0.905	0.07	0.15	460.3	0.098	0.71	1.55
12.0	28.0	3052.0	3052.0	37.3	34.2	86.7	462.5	-462.5	0.0374	2.404	0.907	0.07	0.15	461.2	0.098	0.71	1.55
11.9	28.1	3062.9	3062.9	37.4	34.2	86.9	451.5	-451.5	0.0369	2.398	0.909	0.07	0.15	462.1	0.098	0.71	1.56
11.9	28.1	3062.9	3062.9	37.5	34.3	87.1	441.9	-441.9	0.0364	2.392	0.910	0.07	0.15	462.1	0.098	0.71	1.55
11.8	28.2	3073.8	3073.8	37.5	34.4	87.3	432.6	-432.6	0.0359	2.386	0.912	0.07	0.15	463.1	0.098	0.71	1.56
11.7	28.3	3084.7	3084.7	37.6	34.5	87.5	423.4	-423.4	0.0354	2.381	0.914	0.07	0.15	464.0	0.098	0.72	1.56
11.7	28.3	3084.7	3084.7	37.7	34.5	87.7	414.4	-414.4	0.0349	2.374	0.916	0.07	0.15	464.0	0.098	0.72	1.56
11.6	28.4	3095.6	3095.6	37.8	34.6	87.9	404.6	-404.6	0.0344	2.368	0.918	0.07	0.15	464.9	0.098	0.72	1.56
11.5	28.5	3106.5	3106.5	37.9	34.7	88.0	396.0	-396.0	0.0339	2.362	0.920	0.07	0.15	465.8	0.097	0.72	1.56
11.5	28.5	3106.5	3106.5	37.9	34.8	88.2	387.6	-387.6	0.0333	2.356	0.921	0.07	0.15	465.8	0.097	0.72	1.56
11.4	28.6	3117.4	3117.4	38.0	34.8	88.4	379.4	-379.4	0.0329	2.350	0.923	0.07	0.15	466.7	0.097	0.72	1.56
11.4	28.6	3117.4	3117.4	38.1	34.9	88.6	371.3	-371.3	0.0323	2.343	0.924	0.07	0.15	466.7	0.097	0.72	1.56
11.3	28.7	3128.3	3128.3	38.2	35.0	88.8	362.5	-362.5	0.0318	2.336	0.926	0.07	0.15	467.6	0.097	0.72	1.56
11.2	28.8	3139.2	3139.2	38.3	35.1	89.0	354.8	-354.8	0.0313	2.329	0.928	0.07	0.15	468.4	0.097	0.72	1.56
11.2	28.8	3139.2	3139.2	38.4	35.1	89.2	347.3	-347.3	0.0308	2.322	0.929	0.07	0.15	468.4	0.097	0.72	1.56
11.1	28.9	3150.1	3150.1	38.4	35.2	89.4	339.9	-339.9	0.0303	2.316	0.931	0.07	0.15	469.3	0.097	0.72	1.56
11.0	29.0	3161.0	3161.0	38.5	35.3	89.6	332.7	-332.7	0.0298	2.309	0.932	0.07	0.15	470.2	0.097	0.72	1.56
11.0	29.0	3161.0	3161.0	38.6	35.4	89.8	324.8	-324.8	0.0292	2.301	0.934	0.07	0.15	470.2	0.097	0.72	1.56
10.9	29.1	3171.9	3171.9	38.7	35.4	90.0	317.9	-317.9	0.0287	2.294	0.935	0.07	0.15	471.1	0.097	0.73	1.56
10.8	29.2	3182.8	3182.8	38.8	35.5	90.1	291.8	-291.8	0.0282	2.287	0.940	0.07	0.15	472.0	0.096	0.73	1.56
10.8	29.2	3182.8	3182.8	38.8	35.6	90.3	262.2	-262.2	0.0277	2.279	0.946	0.07	0.15	472.0	0.096	0.73	1.57
10.7	29.3	3193.7	3193.7	38.9	35.7	90.5	235.6	-235.6	0.0272	2.271	0.951	0.07	0.15	472.8	0.096	0.73	1.57
10.6	29.4	3204.6	3204.6	39.0	35.7	90.7	208.8	-208.8	0.0266	2.263	0.957	0.07	0.15	473.7	0.096	0.73	1.58

Kingston Closure Project
Analysis for Liquefaction in the Capillary Fringe

Atmospheric Pressure	2116 psf		Moist Unit Weight of Compacted Ash	109 pcf
Unit Weight of Water	62.4 pcf		Void Ratio of Compacted Ash	0.91
Ground Surface Elevation	790 feet		Specific Gravity of Ash	2.31
Phreatic Surface Elevation	750 feet			

Height above Phreatic Surface feet	Depth below Ground Surface feet	Total Vertical Stress psf	Effective Vertical Stress psf	Volumetric Water Content %	Gravimetric Water Content %	Saturation %	Matric Suction psf	Initial Water Pressure psf	Potential Volumetric Strain	Fcomp	Fsuction	CRRsat	CRRunsat	Maximum Cyclic Shear Stress psf	CSR	Saturated FSliq	Unsaturated FSliq
10.6	29.4	3204.6	3204.6	39.1	35.8	90.9	187.6	-187.6	0.0261	2.254	0.961	0.07	0.15	473.7	0.096	0.73	1.58
10.5	29.5	3215.5	3215.5	39.2	35.9	91.1	168.6	-168.6	0.0256	2.246	0.965	0.07	0.15	474.6	0.096	0.73	1.58
10.4	29.6	3226.4	3226.4	39.3	36.0	91.3	151.4	-151.4	0.0251	2.238	0.968	0.07	0.15	475.4	0.096	0.73	1.58
10.4	29.6	3226.4	3226.4	39.3	36.0	91.5	134.2	-134.2	0.0245	2.228	0.972	0.07	0.15	475.4	0.096	0.73	1.58
10.3	29.7	3237.3	3237.3	39.4	36.1	91.7	120.6	-120.6	0.0240	2.220	0.974	0.07	0.15	476.3	0.096	0.73	1.58
10.2	29.8	3248.2	3248.2	39.5	36.2	91.9	108.4	-108.4	0.0235	2.211	0.977	0.07	0.15	477.2	0.095	0.73	1.58
10.2	29.8	3248.2	3248.2	39.6	36.3	92.0	97.4	-97.4	0.0229	2.202	0.979	0.07	0.15	477.2	0.095	0.73	1.58
10.1	29.9	3259.1	3259.1	39.7	36.3	92.2	87.5	-87.5	0.0224	2.193	0.981	0.07	0.15	478.0	0.095	0.73	1.58
10.0	30.0	3270.0	3270.0	39.8	36.4	92.4	77.5	-77.5	0.0219	2.182	0.984	0.07	0.15	478.9	0.095	0.74	1.58
10.0	30.0	3270.0	3270.0	39.8	36.5	92.6	72.5	-72.5	0.0215	2.176	0.985	0.07	0.15	478.9	0.095	0.74	1.58
9.9	30.1	3280.9	3280.9	39.9	36.5	92.7	66.9	-66.9	0.0212	2.169	0.986	0.07	0.15	479.7	0.095	0.74	1.57
9.8	30.2	3291.8	3291.8	39.9	36.6	92.8	62.6	-62.6	0.0208	2.163	0.987	0.07	0.15	480.6	0.095	0.74	1.57
9.8	30.2	3291.8	3291.8	40.0	36.6	93.0	57.8	-57.8	0.0204	2.155	0.988	0.07	0.15	480.6	0.095	0.74	1.57
9.7	30.3	3302.7	3302.7	40.0	36.7	93.1	54.0	-54.0	0.0201	2.149	0.989	0.07	0.15	481.4	0.095	0.74	1.57
9.6	30.4	3313.6	3313.6	40.1	36.7	93.2	49.9	-49.9	0.0197	2.141	0.989	0.07	0.15	482.2	0.095	0.74	1.57
9.6	30.4	3313.6	3313.6	40.1	36.8	93.3	46.6	-46.6	0.0194	2.134	0.990	0.07	0.15	482.2	0.095	0.74	1.56
9.5	30.5	3324.5	3324.5	40.2	36.8	93.5	43.0	-43.0	0.0190	2.126	0.991	0.07	0.15	483.1	0.094	0.74	1.56
9.4	30.6	3335.4	3335.4	40.3	36.9	93.6	39.7	-39.7	0.0186	2.118	0.992	0.07	0.15	483.9	0.094	0.74	1.56
9.4	30.6	3335.4	3335.4	40.3	36.9	93.7	37.1	-37.1	0.0183	2.111	0.992	0.07	0.15	483.9	0.094	0.74	1.55
9.3	30.7	3346.3	3346.3	40.4	37.0	93.9	34.3	-34.3	0.0179	2.102	0.993	0.07	0.15	484.7	0.094	0.74	1.55
9.3	30.7	3346.3	3346.3	40.4	37.0	94.0	32.0	-32.0	0.0176	2.094	0.993	0.07	0.15	484.7	0.094	0.74	1.55
9.2	30.8	3357.2	3357.2	40.5	37.1	94.1	29.6	-29.6	0.0172	2.086	0.994	0.07	0.15	485.5	0.094	0.74	1.54
9.1	30.9	3368.1	3368.1	40.5	37.1	94.2	27.7	-27.7	0.0169	2.078	0.994	0.07	0.14	486.4	0.094	0.75	1.54
9.1	30.9	3368.1	3368.1	40.6	37.2	94.4	25.5	-25.5	0.0165	2.068	0.995	0.07	0.14	486.4	0.094	0.75	1.53
9.0	31.0	3379.0	3379.0	40.6	37.2	94.5	23.9	-23.9	0.0161	2.061	0.995	0.07	0.14	487.2	0.094	0.75	1.53
8.9	31.1	3389.9	3389.9	40.7	37.3	94.6	22.0	-22.0	0.0158	2.051	0.995	0.07	0.14	488.0	0.094	0.75	1.53
8.9	31.1	3389.9	3389.9	40.7	37.3	94.7	20.6	-20.6	0.0154	2.042	0.996	0.07	0.14	488.0	0.094	0.75	1.52
8.8	31.2	3400.8	3400.8	40.8	37.4	94.9	19.0	-19.0	0.0150	2.032	0.996	0.07	0.14	488.8	0.093	0.75	1.52
8.7	31.3	3411.7	3411.7	40.9	37.4	95.0	17.8	-17.8	0.0147	2.024	0.996	0.07	0.14	489.6	0.093	0.75	1.51
8.7	31.3	3411.7	3411.7	40.9	37.5	95.1	16.4	-16.4	0.0143	2.012	0.997	0.07	0.14	489.6	0.093	0.75	1.50
8.6	31.4	3422.6	3422.6	41.0	37.5	95.3	15.3	-15.3	0.0140	2.003	0.997	0.07	0.14	490.4	0.093	0.75	1.50
8.5	31.5	3433.5	3433.5	41.0	37.6	95.4	14.2	-14.2	0.0136	1.992	0.997	0.07	0.14	491.2	0.093	0.75	1.50
8.5	31.5	3433.5	3433.5	41.1	37.6	95.5	13.2	-13.2	0.0132	1.982	0.997	0.07	0.14	491.2	0.093	0.75	1.49
8.4	31.6	3444.4	3444.4	41.1	37.7	95.7	12.2	-12.2	0.0128	1.970	0.997	0.07	0.14	492.0	0.093	0.75	1.48
8.3	31.7	3455.3	3455.3	41.2	37.7	95.8	11.3	-11.3	0.0124	1.958	0.998	0.07	0.14	492.8	0.093	0.76	1.48
8.3	31.7	3455.3	3455.3	41.2	37.8	95.9	10.6	-10.6	0.0121	1.947	0.998	0.07	0.14	492.8	0.093	0.76	1.47
8.2	31.8	3466.2	3466.2	41.3	37.8	96.0	9.7	-9.7	0.0117	1.935	0.998	0.07	0.14	493.6	0.093	0.76	1.46
8.1	31.9	3477.1	3477.1	41.4	37.9	96.2	9.1	-9.1	0.0114	1.924	0.998	0.07	0.13	494.4	0.092	0.76	1.45
8.1	31.9	3477.1	3477.1	41.4	37.9	96.3	8.4	-8.4	0.0110	1.909	0.998	0.07	0.13	494.4	0.092	0.76	1.44
8.0	32.0	3488.0	3488.0	41.5	38.0	96.4	7.9	-7.9	0.0106	1.898	0.998	0.07	0.13	495.2	0.092	0.76	1.44
7.9	32.1	3498.9	3498.9	41.5	38.0	96.5	7.3	-7.3	0.0103	1.886	0.999	0.07	0.13	496.0	0.092	0.76	1.43
7.9	32.1	3498.9	3498.9	41.6	38.1	96.6	7.0	-7.0	0.0100	1.875	0.999	0.07	0.13	496.0	0.092	0.76	1.42
7.8	32.2	3509.8	3509.8	41.6	38.1	96.7	6.7	-6.7	0.0098	1.868	0.999	0.07	0.13	496.8	0.092	0.76	1.42
7.7	32.3	3520.7	3520.7	41.6	38.1	96.8	6.4	-6.4	0.0096	1.861	0.999	0.07	0.13	497.6	0.092	0.76	1.42
7.7	32.3	3520.7	3520.7	41.7	38.2	96.9	6.1	-6.1	0.0093	1.850	0.999	0.07	0.13	497.6	0.092	0.76	1.41
7.6	32.4	3531.6	3531.6	41.7	38.2	96.9	5.9	-5.9	0.0091	1.842	0.999	0.07	0.13	498.3	0.092	0.76	1.40

Kingston Closure Project
Analysis for Liquefaction in the Capillary Fringe

Atmospheric Pressure	2116 psf		Moist Unit Weight of Compacted Ash	109 pcf
Unit Weight of Water	62.4 pcf		Void Ratio of Compacted Ash	0.91
Ground Surface Elevation	790 feet		Specific Gravity of Ash	2.31
Phreatic Surface Elevation	750 feet			

Height above Phreatic Surface feet	Depth below Ground Surface feet	Total Vertical Stress psf	Effective Vertical Stress psf	Volumetric Water Content %	Gravimetric Water Content %	Saturation %	Matric Suction psf	Initial Water Pressure psf	Potential Volumetric Strain	Fcomp	Fsuction	CRRsat	CRRunsat	Maximum Cyclic Shear Stress psf	CSR	Saturated FSliq	Unsaturated FSliq
7.5	32.5	3542.5	3542.5	41.7	38.2	97.0	5.6	-5.6	0.0089	1.834	0.999	0.07	0.13	499.1	0.092	0.76	1.40
7.5	32.5	3542.5	3542.5	41.8	38.2	97.1	5.3	-5.3	0.0087	1.822	0.999	0.07	0.13	499.1	0.092	0.76	1.39
7.4	32.6	3553.4	3553.4	41.8	38.3	97.2	5.1	-5.1	0.0085	1.813	0.999	0.07	0.13	499.9	0.091	0.77	1.39
7.3	32.7	3564.3	3564.3	41.8	38.3	97.2	4.9	-4.9	0.0083	1.805	0.999	0.07	0.13	500.6	0.091	0.77	1.38
7.3	32.7	3564.3	3564.3	41.9	38.3	97.3	4.7	-4.7	0.0080	1.792	0.999	0.07	0.13	500.6	0.091	0.77	1.37
7.2	32.8	3575.2	3575.2	41.9	38.4	97.4	4.5	-4.5	0.0078	1.783	0.999	0.07	0.12	501.4	0.091	0.77	1.37
7.2	32.8	3575.2	3575.2	41.9	38.4	97.5	4.3	-4.3	0.0076	1.773	0.999	0.07	0.12	501.4	0.091	0.77	1.36
7.1	32.9	3586.1	3586.1	41.9	38.4	97.5	4.1	-4.1	0.0074	1.764	0.999	0.07	0.12	502.2	0.091	0.77	1.36
7.0	33.0	3597.0	3597.0	42.0	38.5	97.6	3.9	-3.9	0.0071	1.750	0.999	0.07	0.12	502.9	0.091	0.77	1.35
7.0	33.0	3597.0	3597.0	42.0	38.5	97.7	3.8	-3.8	0.0069	1.740	0.999	0.07	0.12	502.9	0.091	0.77	1.34
6.9	33.1	3607.9	3607.9	42.0	38.5	97.8	3.6	-3.6	0.0067	1.729	0.999	0.07	0.12	503.7	0.091	0.77	1.33
6.8	33.2	3618.8	3618.8	42.1	38.6	97.9	3.4	-3.4	0.0064	1.714	0.999	0.07	0.12	504.4	0.091	0.77	1.32
6.8	33.2	3618.8	3618.8	42.1	38.6	97.9	3.3	-3.3	0.0062	1.703	0.999	0.07	0.12	504.4	0.091	0.77	1.31
6.7	33.3	3629.7	3629.7	42.1	38.6	98.0	3.2	-3.2	0.0060	1.691	0.999	0.07	0.12	505.2	0.090	0.77	1.31
6.6	33.4	3640.6	3640.6	42.2	38.6	98.1	3.0	-3.0	0.0057	1.675	0.999	0.07	0.12	505.9	0.090	0.77	1.30
6.6	33.4	3640.6	3640.6	42.2	38.7	98.2	2.9	-2.9	0.0055	1.663	0.999	0.07	0.12	505.9	0.090	0.77	1.29
6.5	33.5	3651.5	3651.5	42.2	38.7	98.2	2.8	-2.8	0.0053	1.650	0.999	0.07	0.12	506.7	0.090	0.78	1.28
6.4	33.6	3662.4	3662.4	42.3	38.7	98.3	2.6	-2.6	0.0051	1.632	0.999	0.07	0.11	507.4	0.090	0.78	1.27
6.4	33.6	3662.4	3662.4	42.3	38.8	98.4	2.5	-2.5	0.0048	1.618	1.000	0.07	0.11	507.4	0.090	0.78	1.26
6.3	33.7	3673.3	3673.3	42.3	38.8	98.5	2.4	-2.4	0.0046	1.604	1.000	0.07	0.11	508.2	0.090	0.78	1.25
6.2	33.8	3684.2	3684.2	42.4	38.8	98.5	2.4	-2.4	0.0045	1.594	1.000	0.07	0.11	508.9	0.090	0.78	1.24
6.2	33.8	3684.2	3684.2	42.4	38.8	98.6	2.3	-2.3	0.0044	1.584	1.000	0.07	0.11	508.9	0.090	0.78	1.23
6.1	33.9	3695.1	3695.1	42.4	38.8	98.6	2.2	-2.2	0.0042	1.574	1.000	0.07	0.11	509.6	0.090	0.78	1.23
6.0	34.0	3706.0	3706.0	42.4	38.9	98.7	2.2	-2.2	0.0041	1.563	1.000	0.07	0.11	510.4	0.090	0.78	1.22
6.0	34.0	3706.0	3706.0	42.4	38.9	98.7	2.1	-2.1	0.0039	1.552	1.000	0.07	0.11	510.4	0.090	0.78	1.21
5.9	34.1	3716.9	3716.9	42.5	38.9	98.7	2.1	-2.1	0.0039	1.547	1.000	0.07	0.11	511.1	0.089	0.78	1.21
5.8	34.2	3727.8	3727.8	42.5	38.9	98.8	2.0	-2.0	0.0037	1.536	1.000	0.07	0.11	511.8	0.089	0.78	1.20
5.8	34.2	3727.8	3727.8	42.5	38.9	98.8	2.0	-2.0	0.0036	1.524	1.000	0.07	0.11	511.8	0.089	0.78	1.20
5.7	34.3	3738.7	3738.7	42.5	38.9	98.9	1.9	-1.9	0.0035	1.512	1.000	0.07	0.11	512.6	0.089	0.79	1.19
5.6	34.4	3749.6	3749.6	42.5	39.0	98.9	1.9	-1.9	0.0033	1.500	1.000	0.07	0.10	513.3	0.089	0.79	1.18
5.6	34.4	3749.6	3749.6	42.6	39.0	99.0	1.8	-1.8	0.0032	1.487	1.000	0.07	0.10	513.3	0.089	0.79	1.17
5.5	34.5	3760.5	3760.5	42.6	39.0	99.0	1.8	-1.8	0.0030	1.474	1.000	0.07	0.10	514.0	0.089	0.79	1.16
5.4	34.6	3771.4	3771.4	42.6	39.0	99.0	1.7	-1.7	0.0029	1.461	1.000	0.07	0.10	514.7	0.089	0.79	1.15
5.4	34.6	3771.4	3771.4	42.6	39.0	99.1	1.7	-1.7	0.0028	1.454	1.000	0.07	0.10	514.7	0.089	0.79	1.15
5.3	34.7	3782.3	3782.3	42.6	39.0	99.1	1.7	-1.7	0.0027	1.440	1.000	0.07	0.10	515.4	0.089	0.79	1.14
5.2	34.8	3793.2	3793.2	42.6	39.1	99.2	1.6	-1.6	0.0026	1.426	1.000	0.07	0.10	516.1	0.088	0.79	1.13
5.2	34.8	3793.2	3793.2	42.7	39.1	99.2	1.6	-1.6	0.0024	1.410	1.000	0.07	0.10	516.1	0.088	0.79	1.12
5.1	34.9	3804.1	3804.1	42.7	39.1	99.3	1.5	-1.5	0.0023	1.395	1.000	0.07	0.10	516.8	0.088	0.79	1.11
5.1	34.9	3804.1	3804.1	42.7	39.1	99.3	1.5	-1.5	0.0021	1.378	1.000	0.07	0.10	516.8	0.088	0.79	1.09
5.0	35.0	3815.0	3815.0	42.7	39.1	99.3	1.5	-1.5	0.0020	1.361	1.000	0.07	0.10	517.5	0.088	0.79	1.08
4.9	35.1	3825.9	3825.9	42.7	39.1	99.4	1.4	-1.4	0.0019	1.353	1.000	0.07	0.09	518.3	0.088	0.80	1.08
4.9	35.1	3825.9	3825.9	42.7	39.2	99.4	1.4	-1.4	0.0019	1.344	1.000	0.07	0.09	518.3	0.088	0.80	1.07
4.8	35.2	3836.8	3836.8	42.8	39.2	99.4	1.4	-1.4	0.0018	1.335	1.000	0.07	0.09	519.0	0.088	0.80	1.06
4.7	35.3	3847.7	3847.7	42.8	39.2	99.4	1.4	-1.4	0.0017	1.325	1.000	0.07	0.09	519.6	0.088	0.80	1.06
4.7	35.3	3847.7	3847.7	42.8	39.2	99.5	1.4	-1.4	0.0016	1.316	1.000	0.07	0.09	519.6	0.088	0.80	1.05
4.6	35.4	3858.6	3858.6	42.8	39.2	99.5	1.3	-1.3	0.0016	1.306	1.000	0.07	0.09	520.3	0.088	0.80	1.04

Kingston Closure Project
Analysis for Liquefaction in the Capillary Fringe

Atmospheric Pressure	2116 psf		Moist Unit Weight of Compacted Ash	109 pcf
Unit Weight of Water	62.4 pcf		Void Ratio of Compacted Ash	0.91
Ground Surface Elevation	790 feet		Specific Gravity of Ash	2.31
Phreatic Surface Elevation	750 feet			

Height above Phreatic Surface feet	Depth below Ground Surface feet	Total Vertical Stress psf	Effective Vertical Stress psf	Volumetric Water Content %	Gravimetric Water Content %	Saturation %	Matric Suction psf	Initial Water Pressure psf	Potential Volumetric Strain	Fcomp	Fsuction	CRRsat	CRRunsat	Maximum Cyclic Shear Stress psf	CSR	Saturated FSliq	Unsaturated FSliq
4.5	35.5	3869.5	3869.5	42.8	39.2	99.5	1.3	-1.3	0.0015	1.296	1.000	0.07	0.09	521.0	0.088	0.80	1.04
4.5	35.5	3869.5	3869.5	42.8	39.2	99.5	1.3	-1.3	0.0014	1.286	1.000	0.07	0.09	521.0	0.088	0.80	1.03
4.4	35.6	3880.4	3880.4	42.8	39.2	99.6	1.3	-1.3	0.0014	1.275	1.000	0.07	0.09	521.7	0.087	0.80	1.02
4.3	35.7	3891.3	3891.3	42.8	39.2	99.6	1.3	-1.3	0.0013	1.265	1.000	0.07	0.09	522.4	0.087	0.80	1.01
4.3	35.7	3891.3	3891.3	42.8	39.2	99.6	1.3	-1.3	0.0012	1.254	1.000	0.07	0.09	522.4	0.087	0.80	1.01
4.2	35.8	3902.2	3902.2	42.8	39.2	99.6	1.2	-1.2	0.0011	1.242	1.000	0.07	0.09	523.1	0.087	0.80	1.00
4.1	35.9	3913.1	3913.1	42.9	39.3	99.7	1.2	-1.2	0.0011	1.231	1.000	0.07	0.09	523.8	0.087	0.80	0.99
4.1	35.9	3913.1	3913.1	42.9	39.3	99.7	1.2	-1.2	0.0010	1.219	1.000	0.07	0.09	523.8	0.087	0.80	0.98
4.0	36.0	3924.0	3924.0	42.9	39.3	99.7	1.2	-1.2	0.0009	1.206	1.000	0.07	0.08	524.5	0.087	0.81	0.97
3.9	36.1	3934.9	3934.9	42.9	39.3	99.7	1.2	-1.2	0.0009	1.194	1.000	0.07	0.08	525.1	0.087	0.81	0.96
3.9	36.1	3934.9	3934.9	42.9	39.3	99.7	1.2	-1.2	0.0009	1.194	1.000	0.07	0.08	525.1	0.087	0.81	0.96
3.8	36.2	3945.8	3945.8	42.9	39.3	99.7	1.2	-1.2	0.0008	1.181	1.000	0.07	0.08	525.8	0.087	0.81	0.95
3.7	36.3	3956.7	3956.7	42.9	39.3	99.8	1.1	-1.1	0.0007	1.167	1.000	0.07	0.08	526.5	0.086	0.81	0.94
3.7	36.3	3956.7	3956.7	42.9	39.3	99.8	1.1	-1.1	0.0007	1.167	1.000	0.07	0.08	526.5	0.086	0.81	0.94
3.6	36.4	3967.6	3967.6	42.9	39.3	99.8	1.1	-1.1	0.0007	1.153	1.000	0.07	0.08	527.2	0.086	0.81	0.93
3.5	36.5	3978.5	3978.5	42.9	39.3	99.8	1.1	-1.1	0.0007	1.153	1.000	0.07	0.08	527.8	0.086	0.81	0.94
3.5	36.5	3978.5	3978.5	42.9	39.3	99.8	1.1	-1.1	0.0006	1.139	1.000	0.07	0.08	527.8	0.086	0.81	0.92
3.4	36.6	3989.4	3989.4	42.9	39.3	99.8	1.1	-1.1	0.0006	1.139	1.000	0.07	0.08	528.5	0.086	0.81	0.93
3.3	36.7	4000.3	4000.3	42.9	39.3	99.8	1.1	-1.1	0.0005	1.124	1.000	0.07	0.08	529.2	0.086	0.81	0.91
3.3	36.7	4000.3	4000.3	42.9	39.3	99.9	1.1	-1.1	0.0004	1.108	1.000	0.07	0.08	529.2	0.086	0.81	0.90
3.2	36.8	4011.2	4011.2	42.9	39.3	99.9	1.1	-1.1	0.0004	1.108	1.000	0.07	0.08	529.8	0.086	0.82	0.90
3.1	36.9	4022.1	4022.1	43.0	39.3	99.9	1.1	-1.1	0.0004	1.092	1.000	0.07	0.08	530.5	0.086	0.82	0.89
3.1	36.9	4022.1	4022.1	43.0	39.3	99.9	1.1	-1.1	0.0004	1.092	1.000	0.07	0.08	530.5	0.086	0.82	0.89
3.0	37.0	4033.0	4033.0	43.0	39.3	99.9	1.1	-1.1	0.0004	1.092	1.000	0.07	0.08	531.1	0.086	0.82	0.89
3.0	37.0	4033.0	4033.0	43.0	39.4	99.9	1.1	-1.1	0.0003	1.075	1.000	0.07	0.08	531.1	0.086	0.82	0.88
2.9	37.1	4043.9	4043.9	43.0	39.4	99.9	1.1	-1.1	0.0003	1.075	1.000	0.07	0.08	531.8	0.085	0.82	0.88
2.8	37.2	4054.8	4054.8	43.0	39.4	99.9	1.1	-1.1	0.0003	1.075	1.000	0.07	0.08	532.5	0.085	0.82	0.88
2.8	37.2	4054.8	4054.8	43.0	39.4	99.9	1.0	-1.0	0.0002	1.058	1.000	0.07	0.07	532.5	0.085	0.82	0.87
2.7	37.3	4065.7	4065.7	43.0	39.4	99.9	1.0	-1.0	0.0002	1.058	1.000	0.07	0.07	533.1	0.085	0.82	0.87
2.6	37.4	4076.6	4076.6	43.0	39.4	99.9	1.0	-1.0	0.0002	1.058	1.000	0.07	0.07	533.7	0.085	0.82	0.87
2.6	37.4	4076.6	4076.6	43.0	39.4	99.9	1.0	-1.0	0.0002	1.058	1.000	0.07	0.07	533.7	0.085	0.82	0.87
2.5	37.5	4087.5	4087.5	43.0	39.4	100.0	1.0	-1.0	0.0001	1.039	1.000	0.07	0.07	534.4	0.085	0.82	0.86
2.4	37.6	4098.4	4098.4	43.0	39.4	100.0	1.0	-1.0	0.0001	1.039	1.000	0.07	0.07	535.0	0.085	0.82	0.86
2.4	37.6	4098.4	4098.4	43.0	39.4	100.0	1.0	-1.0	0.0001	1.039	1.000	0.07	0.07	535.0	0.085	0.82	0.86
2.3	37.7	4109.3	4109.3	43.0	39.4	100.0	1.0	-1.0	0.0001	1.039	1.000	0.07	0.07	535.7	0.085	0.83	0.86
2.2	37.8	4120.2	4120.2	43.0	39.4	100.0	1.0	-1.0	0.0001	1.039	1.000	0.07	0.07	536.3	0.085	0.83	0.86
2.2	37.8	4120.2	4120.2	43.0	39.4	100.0	1.0	-1.0	0.0001	1.020	1.000	0.07	0.07	536.3	0.085	0.83	0.84
2.1	37.9	4131.1	4131.1	43.0	39.4	100.0	1.0	-1.0	0.0001	1.020	1.000	0.07	0.07	537.0	0.084	0.83	0.85
2.0	38.0	4142.0	4142.0	43.0	39.4	100.0	1.0	-1.0	0.0001	1.020	1.000	0.07	0.07	537.6	0.084	0.83	0.85
2.0	38.0	4142.0	4142.0	43.0	39.4	100.0	1.0	-1.0	0.0001	1.020	1.000	0.07	0.07	537.6	0.084	0.83	0.85
1.9	38.1	4152.9	4152.9	43.0	39.4	100.0	1.0	-1.0	0.0001	1.020	1.000	0.07	0.07	538.2	0.084	0.83	0.85
1.8	38.2	4163.8	4163.8	43.0	39.4	100.0	1.0	-1.0	0.0001	1.020	1.000	0.07	0.07	538.9	0.084	0.83	0.85
1.8	38.2	4163.8	4163.8	43.0	39.4	100.0	1.0	-1.0	0.0001	1.020	1.000	0.07	0.07	538.9	0.084	0.83	0.85
1.7	38.3	4174.7	4174.7	43.0	39.4	100.0	1.0	-1.0	0.0001	1.020	1.000	0.07	0.07	539.5	0.084	0.83	0.85
1.6	38.4	4185.6	4185.6	43.0	39.4	100.0	1.0	-1.0	0.0001	1.020	1.000	0.07	0.07	540.1	0.084	0.83	0.85
1.6	38.4	4185.6	4185.6	43.0	39.4	100.0	1.0	-1.0	0.0000	1.000	1.000	0.07	0.07	540.1	0.084	0.83	0.83

Kingston Closure Project
Analysis for Liquefaction in the Capillary Fringe

Atmospheric Pressure	2116 psf		Moist Unit Weight of Compacted Ash	109 pcf
Unit Weight of Water	62.4 pcf		Void Ratio of Compacted Ash	0.91
Ground Surface Elevation	790 feet		Specific Gravity of Ash	2.31
Phreatic Surface Elevation	750 feet			

Height above Phreatic Surface feet	Depth below Ground Surface feet	Total Vertical Stress psf	Effective Vertical Stress psf	Volumetric Water Content %	Gravimetric Water Content %	Saturation %	Matric Suction psf	Initial Water Pressure psf	Potential Volumetric Strain	Fcomp	Fsuction	CRRsat	CRRunsat	Maximum Cyclic Shear Stress psf	CSR	Saturated FSliq	Unsaturated FSliq
1.5	38.5	4196.5	4196.5	43.0	39.4	100.0	1.0	-1.0	0.0000	1.000	1.000	0.07	0.07	540.7	0.084	0.84	0.84
1.4	38.6	4207.4	4207.4	43.0	39.4	100.0	1.0	-1.0	0.0000	1.000	1.000	0.07	0.07	541.3	0.084	0.84	0.84
1.4	38.6	4207.4	4207.4	43.0	39.4	100.0	1.0	-1.0	0.0000	1.000	1.000	0.07	0.07	541.3	0.084	0.84	0.84
1.3	38.7	4218.3	4218.3	43.0	39.4	100.0	1.0	-1.0	0.0000	1.000	1.000	0.07	0.07	542.0	0.084	0.84	0.84
1.2	38.8	4229.2	4229.2	43.0	39.4	100.0	1.0	-1.0	0.0000	1.000	1.000	0.07	0.07	542.6	0.083	0.84	0.84
1.2	38.8	4229.2	4229.2	43.0	39.4	100.0	1.0	-1.0	0.0000	1.000	1.000	0.07	0.07	542.6	0.083	0.84	0.84
1.1	38.9	4240.1	4240.1	43.0	39.4	100.0	1.0	-1.0	0.0000	1.000	1.000	0.07	0.07	543.2	0.083	0.84	0.84
1.0	39.0	4251.0	4251.0	43.0	39.4	100.0	1.0	-1.0	0.0000	1.000	1.000	0.07	0.07	543.8	0.083	0.84	0.84
1.0	39.0	4251.0	4251.0	43.0	39.4	100.0	1.0	-1.0	0.0000	1.000	1.000	0.07	0.07	543.8	0.083	0.84	0.84
0.9	39.1	4261.9	4261.9	43.0	39.4	100.0	1.0	-1.0	0.0000	1.000	1.000	0.07	0.07	544.4	0.083	0.84	0.84
0.9	39.1	4261.9	4261.9	43.0	39.4	100.0	1.0	-1.0	0.0000	1.000	1.000	0.07	0.07	544.4	0.083	0.84	0.84
0.8	39.2	4272.8	4272.8	43.0	39.4	100.0	1.0	-1.0	0.0000	1.000	1.000	0.07	0.07	545.0	0.083	0.84	0.84
0.7	39.3	4283.7	4283.7	43.0	39.4	100.0	1.0	-1.0	0.0000	1.000	1.000	0.07	0.07	545.6	0.083	0.85	0.85
0.7	39.3	4283.7	4283.7	43.0	39.4	100.0	1.0	-1.0	0.0000	1.000	1.000	0.07	0.07	545.6	0.083	0.85	0.85
0.6	39.4	4294.6	4294.6	43.0	39.4	100.0	1.0	-1.0	0.0000	1.000	1.000	0.07	0.07	546.2	0.083	0.85	0.85
0.5	39.5	4305.5	4305.5	43.0	39.4	100.0	1.0	-1.0	0.0000	1.000	1.000	0.07	0.07	546.8	0.083	0.85	0.85
0.5	39.5	4305.5	4305.5	43.0	39.4	100.0	1.0	-1.0	0.0000	1.000	1.000	0.07	0.07	546.8	0.083	0.85	0.85
0.4	39.6	4316.4	4316.4	43.0	39.4	100.0	1.0	-1.0	0.0000	1.000	1.000	0.07	0.07	547.4	0.082	0.85	0.85
0.3	39.7	4327.3	4327.3	43.0	39.4	100.0	1.0	-1.0	0.0000	1.000	1.000	0.07	0.07	548.0	0.082	0.85	0.85
0.3	39.7	4327.3	4327.3	43.0	39.4	100.0	1.0	-1.0	0.0000	1.000	1.000	0.07	0.07	548.0	0.082	0.85	0.85
0.2	39.8	4338.2	4338.2	43.0	39.4	100.0	1.0	-1.0	0.0000	1.000	1.000	0.07	0.07	548.6	0.082	0.85	0.85
0.1	39.9	4349.1	4349.1	43.0	39.4	100.0	1.0	-1.0	0.0000	1.000	1.000	0.07	0.07	549.2	0.082	0.85	0.85
0.1	39.9	4349.1	4349.1	43.0	39.4	100.0	1.0	-1.0	0.0000	1.000	1.000	0.07	0.07	549.2	0.082	0.85	0.85
0.0	40.0	4360.0	4360.0	43.0	39.4	100.0	1.0	-1.0	0.0000	1.000	1.000	0.07	0.07	549.8	0.082	0.85	0.85